Bellotti, R. *et al.* (1989). *Géotechnique* **39**, No. 2, 269–292

Interpretation of moduli from self-boring pressuremeter tests in sand

R. BELLOTTI*, V. GHIONNA†, M. JAMIOLKOWSKI†,
P. K. ROBERTSON‡ and R. W. PETERSON§

The pressuremeter is a unique method for assessing directly the in situ shear stiffness of soils. However, the correct interpretation and application of the measured modulus must account for the relevant stress and strain level acting around the pressuremeter during the test. A method to correct the measured unload–reload shear modulus from self-bored pressuremeter tests in sands is proposed. The method has been evaluated using extensive data obtained from 47 tests performed in a large calibration chamber using pluvially-deposited silica sand and from 25 tests performed in situ in a natural deposit of relatively clean silica sand at the River Po, Italy. A consistent relationship was obtained between the corrected unload–reload shear modulus and the small strain shear modulus determined from resonant column tests and field cross-hole tests. Suggestions are given to link the measured moduli with moduli values required for geotechnical design problems. The importance of strain level, stress-strain model, yield and number of load cycles is discussed.

KEYWORDS: analysis; field tests; sands; shear modulus; site investigation; stiffness.

Le pressiomètre représente une méthode unique pour évaluer directement in situ la rigidité en cisaillement des sols. L'interprétation correcte et l'application du module mesuré doivent expliquer le niveau exact des contraintes et des déformations agissant autour du pressiomètre pendant l'essai. L'article propose une méthode pour corriger le module mesuré de cisaillement déchargement-rechargement à partir d'essais au pressiomètre auto foreur dans des sables. La méthode fut etablie sur la base de données detaillées obtenues par 47 essais effectués dans une grande chambre d'étalonnage en employant du sable silicieux deposée en pluie et de 25 essais effectués in situ dans un dépôt naturel de sable silicieux relativement propre du Pô (Italie). Une relation constante fut obtenue entre le modèle corrigé de cisaillement déchargement-rechargement et le module bas de cisaillement de déformation déterminé à partir d'essais de colonne résonante et d'essais à trous croisés sur chantier. L'article donne des suggestions pour relier les modules mesurés aux valeurs modulaires nécessaires pour des problèmes de construction géotechniques. On discute l'importance du niveau de déformation, le modèle des contraintes et des déformations, le déplacement et le nombre de cycles de chargement.

NOTATION

a	cavity radius at start of loop
BC, CC	boundary conditions
D	diameter of pressuremeter
D_R	relative density
D_{Rc}	relative density after consolidation
D_{50}	mean grain size
E'	drained Young's modulus
$E'(G^{RC})$	E' derived from G^{RC}
F_N	correction factor for number of cycles
G	shear modulus
G_{HH}	shear modulus for shearing in the horizontal plane
G_{HV}	shear modulus for shearing in the vertical plane
G_i	initial tangent shear modulus
G_0	maximum shear modulus
G_0^{CH}	G_0 from seismic cross-hole tests
G_0^{DH}	G_0 from seismic down-hole tests
G_0^{RC}	G_0 from resonant column tests
G_0^{SBP}	G_0 derived from G_{UR} in SBPTs
G_s	secant pressuremeter modulus
$G_s^{1\cdot5}$	G_s at cavity volumetric strain $\Delta V/V_0 = 1{\cdot}5\%$
G_{UR}	secant shear modulus for unload-reload cycle
G_{RU}	secant shear modulus for reload-unload cycle
G_{UR}^c	G_{UR} normalized to the in situ stress level
G_{RU}^c	G_{RU} normalized to the in situ stress level
K_D	dilatometer horizontal stress index
K_0	coefficient of earth pressure at rest

Discussion on this Paper closes on 6 October 1989. For further details see p. ii.

* ENEL-CRIS, Milan.
† Politecnico di Torino.
‡ University of Alberta.
§ US Army Waterways Experiment Station, Vicksburg.

L length of pressuremeter membrane
M_0 constrained modulus
n modulus exponent
N number of tests
N_c number of cycles
N_{SPT} SPT blow count
p, p' total and effective radial stress at the cavity wall, respectively
p_a reference stress; $p_a = 98{\cdot}1$ kPA
p_A, p_A' total and effective cavity stress at the end of unloading, respectively
p_B, p_B' total and effective cavity stress at the closure of cycle, respectively
p_c, p_c' total and effective cavity stress at the start of unloading, respectively
p_0' initial cavity effective stress
p_y' effective radial yield stress
q_c static cone penetration resistance
R radius of cavity
R_0 initial radius of cavity
R_p radius of plastic zone at start of loop
RU reloading–unloading
s' effective mean stress on horizontal plane; $s' = (\sigma_r' + \sigma_\theta')/2$
s_{AV}' average value of s' around cavity
s_0' in situ mean effective stress on horizontal plane
u_0 pore pressure at centre of calibration chamber
UR unloading–reloading
α undimensional factor
β undimensional factor
γ shear strain or shear strain amplitude of the cycle
γ_{AV} average shear strain amplitude of the cycle around the cavity
γ_d bulk density
γ_r reference shear strain
γ_t^e elastic 'threshold', shear strain or shear strain amplitude of the cycle
γ_t^p plastic 'threshold', shear strain or shear strain amplitude of the cycle
γ_{UR} shear strain amplitude of unload-reload cycle
$\Delta p'$ change in cavity effective stress during a cycle
ΔR change in radius of cavity
$\Delta\gamma_c$ shear strain increment during unload-reload or reload-unload cycle at the cavity wall
ε_A pressuremeter cavity strain at end of unloading
ε_B pressuremeter cavity strain at loop closure
ε_C circumferential strain at the cavity wall
ε_h horizontal strain
ε_v vertical strain
ε_θ circumferential strain
ν' Poisson's ratio
ϕ_{PS}' friction angle under plane strain condition
ϕ_{TX}' friction angle under axisymmetric condition
σ_h, σ_h' total and effective horizontal stress, respectively
σ_m' mean effective stress
σ_{mc}' mean effective consolidation stress
σ_r' effective radial stress
σ_v, σ_v' total and effective vertical stress, respectively
σ_θ' effective circumferential stress
σ_{m0}' in situ mean effective stress
τ shear stress
τ_f shear stress at failure
τ_{max} maximum shear stress
1_{SD} standard deviation

INTRODUCTION

The self-boring pressuremeter test (SBPT) is conceptually an ideal in situ test for the determination of engineering properties of soils. It is particularly useful for performing drained tests on sands and sandy soils, since these soils are frequently difficult, if not impossible, to retrieve and test undisturbed, especially when very loose.

One of the most common uses of a SBPT in sand is for the evaluation of the soil moduli (Wroth, 1982). However, the interpretation and application of moduli determined from a SBPT in sand is related to the fact that soil moduli vary with both stress and strain levels. In a pressuremeter test the stresses and strains vary with the radial distance from the probe. The often complex variation of stresses and strains is a common problem for the interpretation of most forms of in situ tests (Jamiolkowski, Ladd, Germaine & Lancellotta, 1985). However, the SBPT has the advantage of well-defined boundary conditions which make it possible to calculate the variation of stresses and strains with relatively simple closed-form solutions.

The early methods for the evaluation of deformation characteristics of soils from the results of a SBPT for design purposes were usually linked to the assumption that the probe was expanded in a linear, isotropic, elastic, perfectly plastic soil. With this simplified assumption the soil surrounding the probe is subjected to pure shear only. This holds true provided the applied pressuremeter cavity effective stress p' stays below the yield stress p_y' of the soil element adjacent to the cavity wall. The values of p_y' in a purely frictional Coulomb material are given by the equation (Baguelin, Jezequel & Shields, 1978; Houlsby, Clarke & Wroth, 1986)

$$p_y' = \sigma_{h0}'(1 + \sin \phi_{PS}') \quad (1)$$

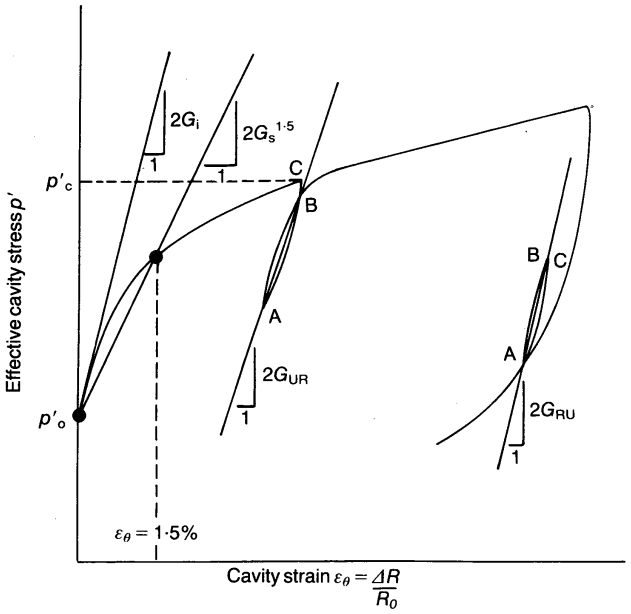

Fig. 1. Shear moduli from SBP tests

where σ_{h0}' is in situ horizontal effective stress (for well-performed SBPTs, $\sigma_{h0}' = p_0'$, where p_0' is initial cavity effective stress), and ϕ_{PS}' is peak friction angle under plain strain conditions.

Within the assumed idealized scheme of soil behaviour shown in Fig. 1, for the range of effective cavity stress $p_0' < p' \leqslant p_y'$ the pressuremeter curve should have a constant slope of $2G_i$, where G_i is the initial tangent shear modulus of the soil. However, since G_i can only be determined with validity from the very early part of the expansion curve, the value is sensitive to soil disturbance due to installation. An alternative approach was proposed by Hughes (1982) and Wroth (1982), in which the 'elastic' shear modulus could be measured by performing small unloading-reloading cycles during a pressuremeter expansion test. If the soil is perfectly elastic in unloading, then the unloading-reloading cycle will have a gradient of $2G_{UR}$, where G_{UR} is the unload-reload shear modulus (Fig. 1).

Wroth (1982) suggested that the amplitude of the unloading should avoid the failure of the soil at the cavity wall in extension. For an isotropic-elastic, perfectly plastic material the magnitude of the change in cavity effective stress $\Delta p'$ during an elastic unloading should therefore not exceed

$$\Delta p' = \frac{2 \sin \phi_{PS}'}{1 + \sin \phi_{PS}'} p_c' \qquad (2)$$

where p_c' is effective stress at which unloading loop starts. Qualitatively, within the framework of elasto-plasticity it can be demonstrated that during a drained test, unloading of the expanding cavity wall after the soil has reached failure will bring the surrounding soil below the current yield surface. Within the yield surface the strains are small and to a large extent recoverable (Fig. 1).

In addition to G_i and G_{UR}, it is also possible to evaluate the secant pressuremeter modulus G_s directly from the expansion curve. The assessment of G_s is based on the assumption of an elastic soil behaviour which, except for the early part of the expansion curve ($p' \leqslant p_y'$) where $G_s \simeq G_i$ and during unloading-reloading cycles, is conceptually not true. Despite this lack of a clear physical meaning, G_s is frequently incorporated in the empirical design rules for shallow and deep foundations in France (Baguelin *et al.*, 1978).

In all soils, and especially sands, the early part of the SBPT is strongly influenced by disturbance due to the installation. Therefore, G_i and G_s are also strongly influenced by disturbance. However, experience (Hughes, 1982; Wroth, 1982; Robertson & Hughes, 1986) has shown that G_{UR} is almost completely independent from the initial shape of the expansion curve, and hence independent from disturbance. Despite this advantage, there still exists the problem of how to apply the measured G_{UR} values in engineering design.

Robertson (1982) and Robertson & Hughes (1986) suggested that G_{UR} should be corrected to account for the average stress and strain level existing around the probe. This Paper proposes a modified method to correct G_{UR} for stress and strain level. The evaluation of the proposed method is made using extensive data obtained from 47 SBPTs performed in the ENEL-CRIS calibration chamber (CC) (Bellotti, Crippa, Ghionna, Jamiolkowski & Robertson, 1987) and from 25 SBPTs performed in the field at a site near the River Po, Italy (Bruzzi, Ghionna, Jamiolkowski, Lancellotta & Manfredini, 1986).

A REVIEW OF SAND BEHAVIOUR

Recent research using the resonant column (Dobry, Powell, Yokel & Ladd, 1980) has shown that below an elastic 'threshold' shear strain (half-cycle amplitude, γ_t^e) the soil behaviour is approximately linear elastic. Fig. 2 presents results on Ticino sand from an undrained resonant column test. Below a shear strain amplitude of about $10^{-3}\%$ the modulus is practically constant and equal to the maximum shear modulus G_0. Between a shear strain amplitude of $10^{-3}\%$ and up to about $6 \times 10^{-3}\%$ the soil behaves non-linearly, with a resulting reduction in shear modulus, although no excess residual pore pressures are generated. The lack of residual pore pressure generation implies that no plastic deformations will take place in drained conditions. Therefore, the start of residual pore pressure development can be postulated in first approx-

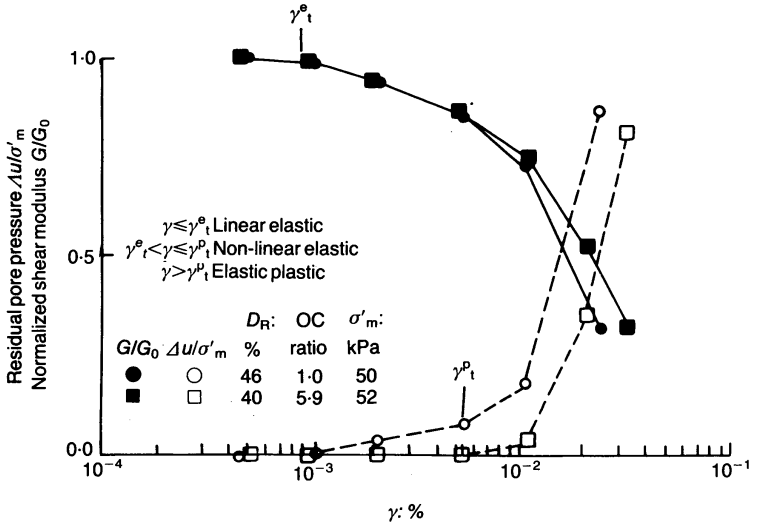

Fig. 2. Behaviour of Ticino sand during resonant column test (adapted from Lo Presti, 1987)

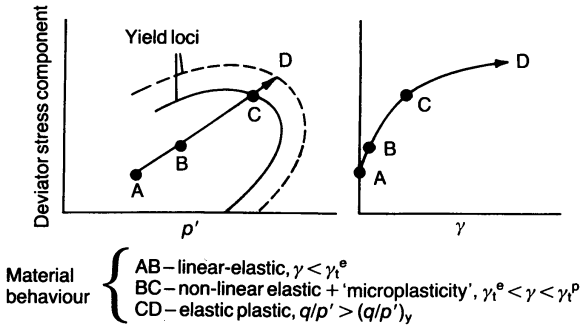

Fig. 3. Qualitative sand behaviour

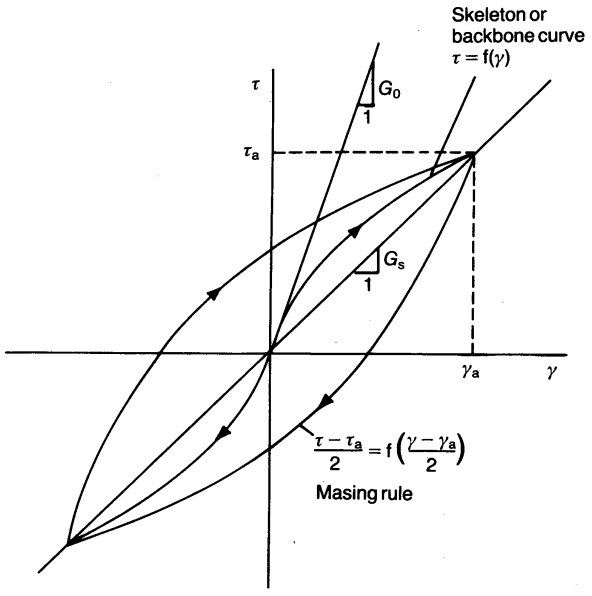

Fig. 4. Simple stress-strain model for cyclic loading of sand (adapted from Hardin & Drnevich, 1972)

imation as a plastic threshold (γ_t^p). Above this plastic threshold ($\gamma > \gamma_t^p$) the qualitative behaviour of the soil will be approximately elastic plastic. This plastic threshold is consistent with the yield stress within the framework of elasto-plasticity. A similar behaviour has been observed in drained resonant column tests on Ticino sand in which a similar elastic threshold (γ_t^e) is observed.

Figure 3 shows qualitatively the idealized elastic-plastic behaviour of sands. Below an elastic threshold ($\gamma \leqslant \gamma_t^e$) the soil is assumed to be linear elastic. With shear strains above the elastic but below the plastic threshold ($\gamma_t^e < \gamma < \gamma_t^p$) the soil is assumed to be non-linear elastic with some microplasticity. Above the plastic threshold or the yield stress, the soil is elastic-plastic.

Laboratory testing (Hardin & Drnevich, 1972) has also shown that during unloading, the unloading stress–strain curve is twice as large as the virgin loading (skeleton or backbone) curve. This phenomenon is usually represented by the Masing rule (Fig. 4).

Figure 5 shows an idealized representation of two possible unloading-reloading cycles for a drained shear test on sand. Following the Masing rule, if the shear strain amplitude during unloading is less than twice the elastic threshold strain ($\gamma_{UR} \leqslant 2\gamma_t^e$) the unload-reload cycle will be linear with a slope equal to the maximum shear modulus ($G_{UR} = G_0$). If the unloading shear strain amplitude is greater than twice the elastic threshold strain ($\gamma_{UR} > 2\gamma_t^e$) the unload-reload loop will be non-linear and hysteretic, and G_{UR} will be less than G_0, approaching G_0 only in the very early part of the unloading branch. However, in both cases the direct determination of G_0 from the

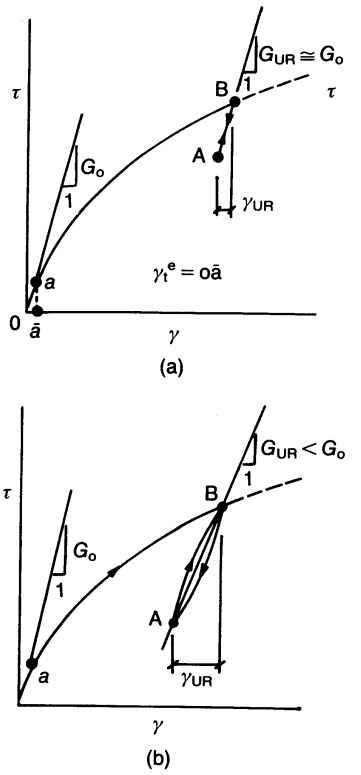

Fig. 5. Idealized drained unloading-reloading loop from SBPT in sand: (a)$\gamma_{UR} \leqslant 2\gamma_t^e$; (b) $\gamma_{UR} \geqslant 2\gamma_t^e$

experimental data is unreliable because of the high precision required in the measurement of the strains. This prerequisite is critical at the stress reversals, where non-linearity and hysteresis of the strain sensors, creep of the soil, etc. can strongly affect the measured values.

In summary, laboratory studies have shown that the following points approximate the behaviour of most sands.

(*a*) Below an elastic threshold shear strain γ_t^e the soil is linear elastic: typically, $\gamma_t^e \simeq 10^{-3}\%$.
(*b*) For shear strains above the elastic threshold strain but below yield or a plastic threshold strain γ_t^p, the soil behaviour can be assumed to be non-linear elastic with possibly some micro-plasticity.
(*c*) If the soil is unloaded with a shear strain amplitude of γ_{UR}, where $\gamma_{UR} < 2\gamma_t^e$, the initial slope of the unloading curve should, in principle, be equal to the maximum shear modulus G_0.
(*d*) If the shear strain amplitude during an unloading-reloading cycle is greater than twice the elastic threshold strain ($\gamma_{UR} > 2\gamma_t^e$), a non-linear hysteretic loop is formed and the unloading curve is approximately twice as large as the skeleton (backbone) stress strain curve as defined by the Masing rule.

SBPT INTERPRETATION

Figure 6 shows a typical high-quality SBPT pressure expansion curve with an unloading-reloading cycle in a clean free-draining sand, and an expanded plot of the first unloading-reloading cycle. The following points are illustrated.

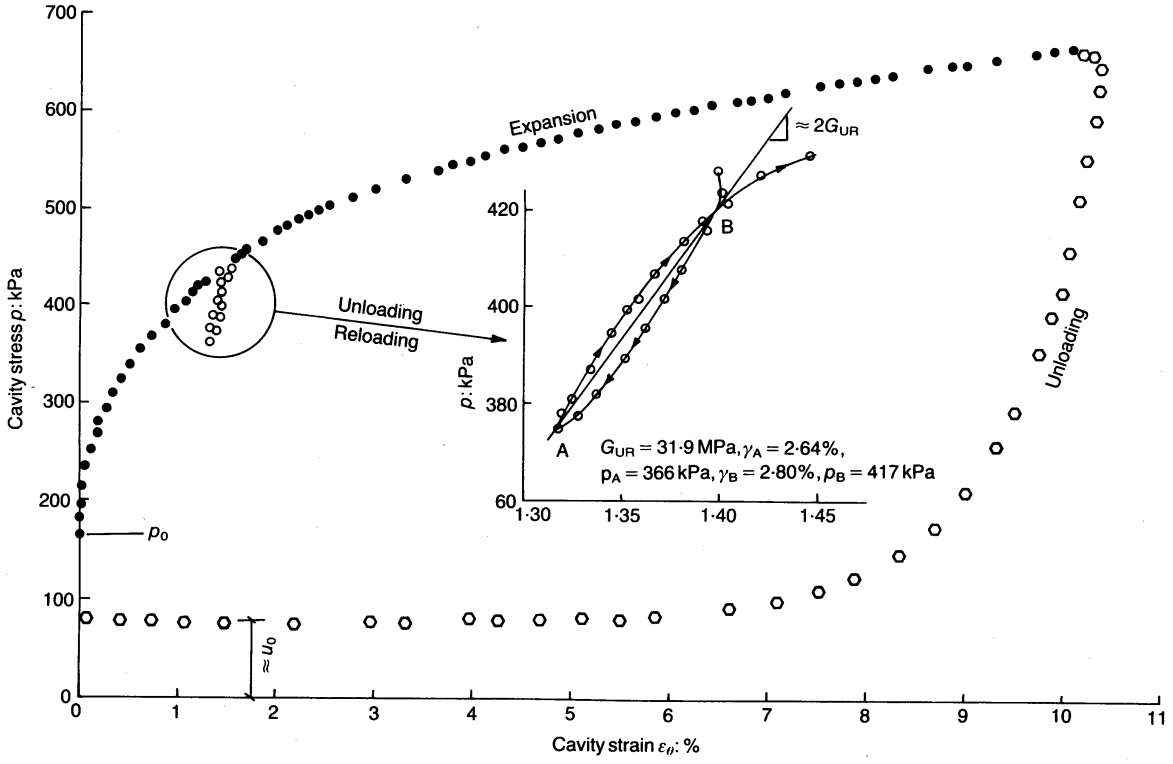

Fig. 6. Example of SBPT in River Po sand (borehole 4017, depth 10·4 m, groundwater level 1·6 m)

(*a*) The pressure expansion curve is highly non-linear and the evaluation of G_i is difficult and subjective.
(*b*) The unloading-reloading cycle has a slope that is considerably steeper than the secant or tangent to the pressure-expansion curve.
(*c*) The unloading-reloading cycle is non-linear.

The importance of creep during pressuremeter tests in sands has been noted (Hughes, 1982; Robertson, 1982; Withers, Howie, Hughes & Robertson, 1988). For pressuremeter testing in clean sands the accumulation of strains (creep) at constant cavity stress is generally not associated with pore pressure dissipation.

The amount of creep deformation increases as the cavity stress increases. Procedures for performing unloading-reloading cycles usually take account of creep deformation by carrying out one of the following procedures.

(*a*) Hold cavity stress constant and record cavity strain ($\Delta R/R_0$) until an acceptably low rate of strain (creep) has been reached, then perform unloading-reloading cycle.
(*b*) Perform unloading-reloading cycle without any holding period, but calculate the slope of the unload-reload cycle between the two apexes of the cycle, as shown in Fig. 6.

Allowing the creep displacements to occur before unloading can provide additional information on the sensitivity of the pressure-expansion curve to the rate of expansion (Withers *et al.*, 1988).

Robertson (1982) and Robertson & Hughes (1986) proposed that the moduli obtained from pressuremeter unloading-reloading loops in sand should be corrected for the average stress and strain level existing around the pressuremeter cavity.

The average stress level may be taken as either the mean octahedral effective stress σ_m' (Robertson, 1982) or the mean value of the plane strain effective stress s' (Fahey & Randolph, 1984). Robertson (1982) proposed that as a first approximation the average mean octahedral effective stress (σ_{AV}') around the cavity can be taken as

$$\sigma_{AV}' \simeq 0{\cdot}5p_c' \tag{3}$$

It was also proposed that the average shear strain amplitude of the cycle around the cavity could be approximated

$$\gamma_{AV} \simeq 0{\cdot}5\Delta\gamma_c \tag{4}$$

where $\Delta\gamma_c$ is the shear strain amplitude of the cycle at the cavity wall $\gamma = 2(\varepsilon_B - \varepsilon_A)$ (see Fig. 6).

With a knowledge of σ_{AV}' it was proposed that the unload-reload modulus could be corrected for stress level $G_{UR}{}^c$ using the formula proposed by Janbu (1963)

$$G_{UR}{}^c = G_{UR}\left(\frac{\sigma_{m0}'}{\sigma_{AV}'}\right)^n \tag{5}$$

where σ_{m0}' is in situ mean effective stress and n is the modulus exponent. For sand, n is generally in the range 0·4–0·5, with a tendency to increase with increasing level of strain (Wroth, Randolph, Houlsby & Fahey, 1979; Iwasaki, Tatsuoka, Tokida & Yasuda, 1978). Using this approach, Robertson & Hughes (1986) compared the pressuremeter unload-reload shear moduli corrected to the in situ mean effective stress $G_{UR}{}^c$ with the small strain shear moduli $G_0{}^{DH}$ computed from shear wave velocities obtained using a downhole seismic cone (Campanella & Robertson, 1984; Robertson, Campanella, Gillespie & Rice, 1986). Their results are summarized in Fig. 7. The shear moduli from the pressuremeter shown in Fig. 7 were determined from small unload-reload loops with a typical shear strain amplitude of the cycle of about 0·2–0·3%. The results indicate a relationship between $G_{UR}{}^c$ from the SBPT and the small strain $G_0{}^{DH}$ of $G_{UR}{}^c/G_0{}^{DH} = 0{\cdot}2$–$0{\cdot}6$.

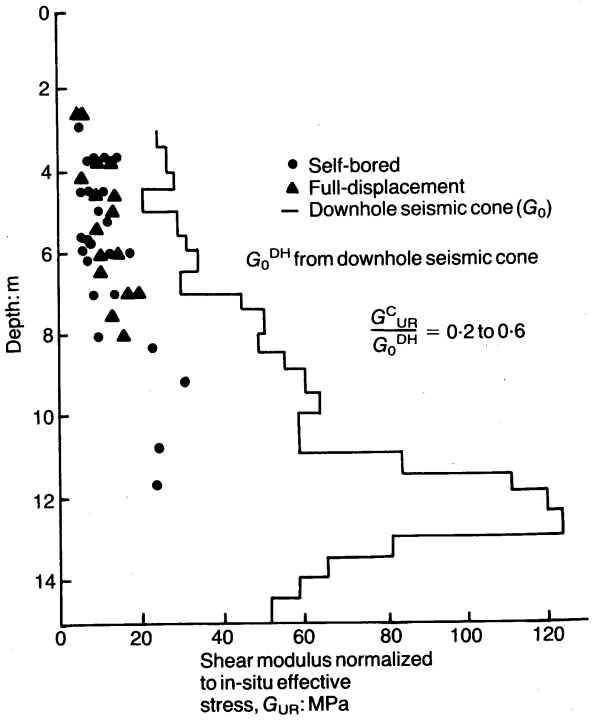

Fig. 7. Comparison of shear moduli from downhole seismic shear wave velocities and shear moduli normalized to in situ effective stress level from self-bored and full-displacement pressuremeter tests (after Robertson & Hughes, 1986)

PROPOSED INTERPRETATION

To provide a more consistent framework for correcting SBPT moduli from unload-reload cycles to account for variations in stress and strain levels, the following method is proposed. The average values of the mean plane strain effective stress s_{AV}' and the shear strain amplitude of the cycle γ_{AV} are calculated within the plastic zone that exists at the start of the unload-reload loop. The radial distribution of σ_r' and σ_θ' in the plastic zone at the start of shear reversal is evaluated from cavity expansion theory, with the simplified assumption of an elastic perfectly plastic soil behaviour. The average shear strain γ_{AV} is calculated from the elastic strain distribution in the same region during the unloading-reloading cycle. The influence of high non-linearity and gradient of stress and strain close to the probe has been incorporated by integrating the shear stresses and strains with the inverse of the current radius. Thus, more weight has been placed on the soil response close to the cavity.

The average plane strain effective stress and shear strain existing in the plastic zone around the probe at the start of the unload-reload loop can be given by

$$s_{AV}' = \sigma_{h0}' + \alpha(p_c' - \sigma_{h0}') \quad (6)$$

$$\gamma_{AV} = \beta\Delta\gamma_c \quad (7)$$

where α and β are reduction factors that are a function of p_0', p_c' and ϕ_{PS}' (Appendix 1). For an elastic perfectly plastic material, these expressions are valid only if a plastic zone has been formed, i.e. when $p' > p_y'$.

In practice, for field testing the true value of σ_{h0}' is generally unknown. Therefore, the evaluation of α and β is made by assuming $\sigma_{h0}' \simeq p_0'$. Usually p_0' is evaluated from the lift-off stress of the SBPT pressure-expansion curve.

If the unload–reload loop is performed before a plastic zone has developed ($p' < p_y'$), it can be assumed that $s_{AV}' \simeq p_0' \simeq \sigma_{h0}'$ and $\gamma_{AV} \simeq \Delta\gamma_c$.

Although the assumptions to calculate the average strain can produce large errors due to the real non-linear soil behaviour, they were considered to be consistent with the overall approach taken to evaluate the average stress and were therefore considered superior to a more complex soil model which would require introduction of additional variables for a numerical solution. The influence of non-linearity is discussed later when dealing with the interpretation.

EVALUATION OF PROPOSED METHOD

Calibration chamber study

In all, 47 SBPTs have been performed in the ENEL-CRIS calibration chamber (Bellotti *et al.*, 1987). The tests were performed in dry and saturated Ticino and Hokksund sand. Pressuremeter tests were performed with the probe in plac during sample preparation (ideal installation) an with the probe self-bored into saturated sanc The purpose of the CC testing was to evaluate th performance of the self-boring pressuremete (SBP) probe under strictly controlled laborator conditions, and to review critically existing inter pretation methods of the SBPT in sands. Th results presented in this Paper form part of larger study (Bellotti *et al.*, 1987).

The ENEL-CRIS calibration chamber wa designed to calibrate and evaluate different in sit testing devices in sands under strictly controlle boundary conditions. A complete description c the chamber was given by Bellotti, Bizzi & Ghionna (1982). The equipment consists of double-wall chamber, a loading frame, a mas sand spreader for sand deposition and a satura tion system. The chamber can test a cylindrica sample of sand 1·2 m in diameter and 1·5 m i height (Fig. 8).

The sample is confined laterally with a flexibl rubber membrane surrounded by water, throug which the horizontal stresses are applied. Th bottom of the sample is supported on a wate filled cushion resting on a rigid steel piston. Th vertical confining stress is applied through th water-filled base cushion, and vertical deflectio of the sample is controlled by the movement c the base steel piston. The top of the sample i confined by a rigid top plate and fixed beam. Th double-walled chamber allows the application c a zero average lateral strain boundary conditio to the test sample by maintaining the pressure i the double-wall cavity equal to the lateral pres sure acting on the sample membrane. The axia and lateral confining pressures can be varie independently, so that the ratio of the applie horizontal stress σ_h to the vertical stress σ_v can b maintained at any desired value.

The SBP probe used in the CC study was th Camkometer Mark VIII, manufactured by Cam bridge In-Situ Ltd. It is essentially a thick-walle steel cylinder with a flexible membrane attache to the outside. The instrument is advanced int the ground as the soil, which is displaced by sharp cutting shoe, is removed from the centre c the probe by the action of a rotating cutter insid the shoe. The cuttings are flushed to the surfac by water or drilling mud which is pumped dow to the cutting head.

The cylindrical adiprene membrane used in th CC study was 82 mm in diameter and 490 mr long, corresponding to a length to diameter rati L/D of approximately 6. The adiprene membran was designed to be flush with the body of th probe. During penetration and testing in dense c abrasive soils, an outer flexible protective mem brane with stainless steel strips ('chinese lantern

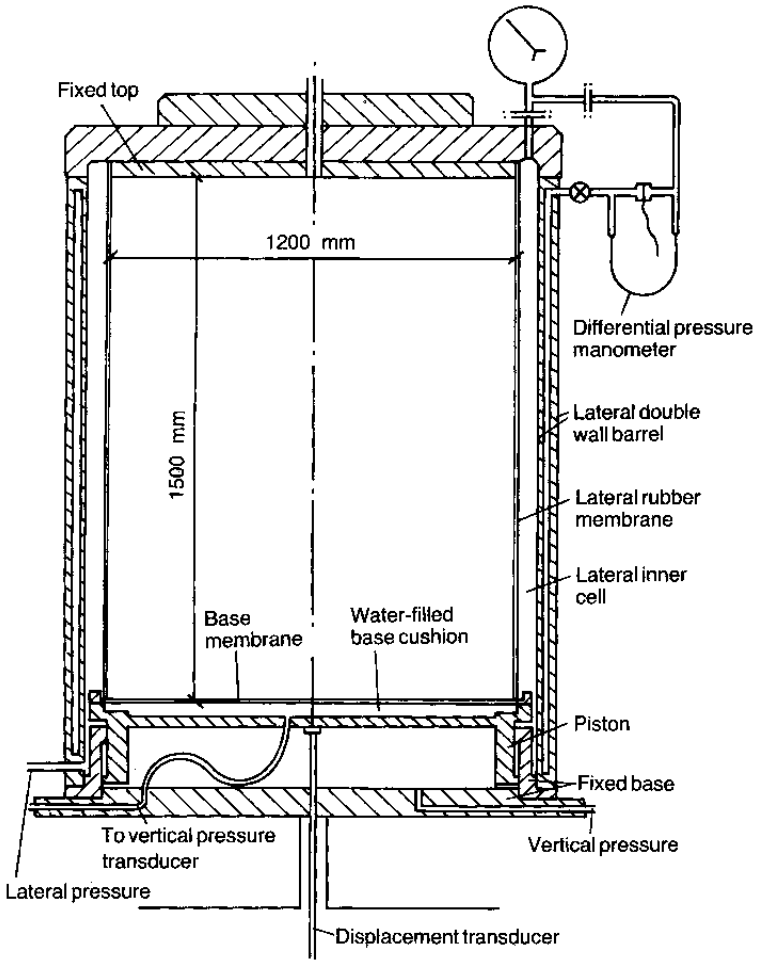

Fig. 8. Cross-section of ENEL-CRIS calibration chamber

can be placed over the adiprene membrane. Once the instrument is at the desired test depth, the membrane is expanded against the soil using pressurized nitrogen gas. The radial expansion of the membrane is measured at the mid-height of the membrane by three pivoted levers, called strain arms. These, which are located at 120° around the circumference, are kept in light contact with the inside of the membrane by strain-gauged cantilever springs. Individual and average readings of the three strain arms were taken.

A strain-gauged total pressure cell is located inside the probe to measure the inflation gas pressure. Two strain-gauged pore pressure cells are also incorporated into the membrane. The data from all six transducers (three strain, one total pressure and two pore pressure) were collected by the data acquisition system, consisting of a data capture unit, a thermal paper printer, a cartridge-equipped HP 9825 computer and a paper tape printer. The output was also recorded on a four-channel y-t chart recorder and an x-y plotter for simultaneous plotting of raw data. The CC loading and data acquisition system are shown in Figs 9 and 10.

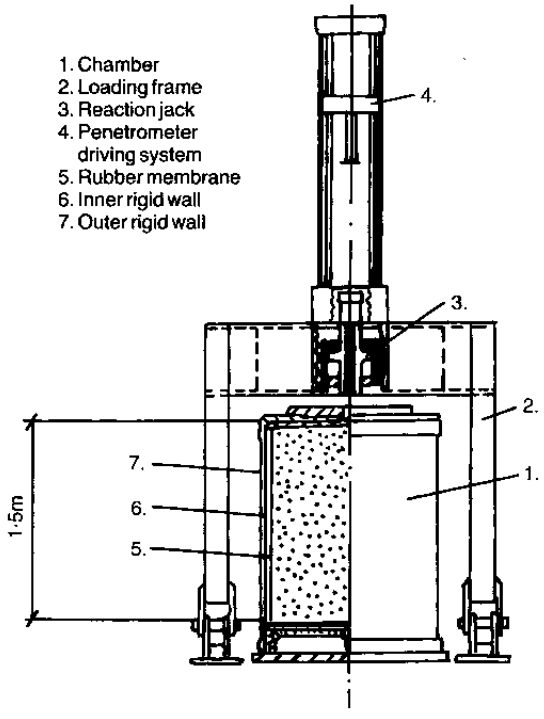

Fig. 9. CC loading system

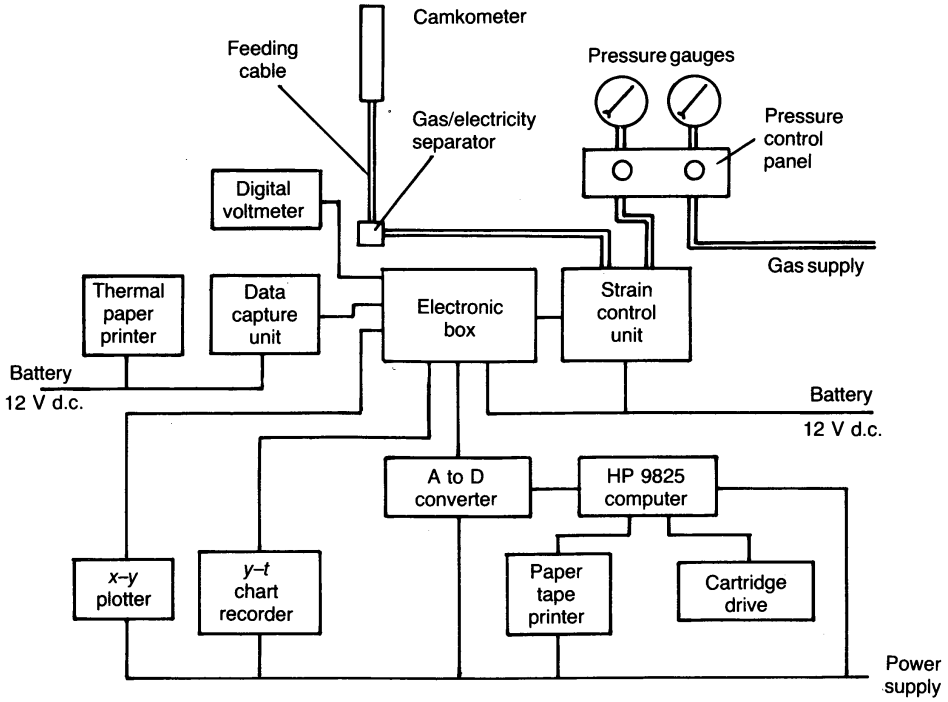

Fig. 10. Data acquisition system for SBPT

Two natural sands were tested: Ticino sand from Italy and Hokksund sand from Norway. Both sands have a uniform gradation and are medium–coarse grained, with a mean grain size $D_{50} = 0{\cdot}53$ mm for Ticino sand and $D_{50} = 0{\cdot}39$ mm for Hokksund sand. A detailed description of the physical properties of the two sands was given by Baldi, Bellotti, Crippa, Fretti, Ghionna, Jamiolkowski, Ostricati, Pasqualini & Pedroni (1985). All test samples were prepared by pluvial deposition of dry sand in air using a gravity mass sand spreader (Jacobsen, 1976). Sample formation was performed in one operation using a sand container which holds enough sand for the specimen preparation. The uniformity of the samples was generally good, although somewhat erratic for medium-dense specimens ($40\% \leqslant D_R \leqslant 60\%$). Full details concerning sample homogeneity were given by Baldi *et al.* (1985).

'Ideal' installation

To evaluate the influence of the self-boring installation on the pressuremeter results a series of tests were performed with 'ideal installation'. The probe was placed in the centre of the CC before sample formation, with the mid-height of the SBP membrane approximately 65 cm from the sample base. A protective cylinder was placed above the probe and extended up to the base of the sand container. This was done to avoid sand falling on to the top of the probe during sample formation.

Self-bored installation

To simulate field self-boring conditions a series of tests were performed with the probe self-bored into the CC. For these tests the sand samples were first formed using pluvial deposition, and then saturated with de-aired water. The probe was self-bored into the CC using water as the flushing fluid. Drainage was allowed at the base of the sample. Installation was performed with various boundary conditions in order to evaluate their influence on the test results. During installation, a small vacuum (50 kPa) was applied to the inside of the SBP probe to maintain the adiprene membrane in close contact with the body of the probe. The probe was advanced into the CC at a rate of about 3 cm/min using a cutter speed which was maintained at a rate of about 60 revolutions/min. The distance of the cutter from the leading edge of the cutting shoe was varied from 1·9 cm to 5·4 cm. The size of the cutting shoe was adjusted to be the same diameter as the membrane. For the tests in dense sand the adiprene membrane was generally protected by using the chinese lantern.

A flowmeter was used to monitor the flow rate of the flushing water sent to the cutter. The flow rate was generally about 9–12 l/min. The flow rates from the probe and calibration drainage lines were also monitored. During the installation, the CC pore pressures and boundary stresses and strains were monitored. All the sand flushed out of the CC during installation was carefully collected and weighed (oven-dry).

Following sample formation and probe installation, the samples were subjected to one-dimensional consolidation under conditions of no average lateral strain (i.e. $\Delta\varepsilon_h = 0$). Normally consolidated (NC) and mechanically overconsolidated (OC) specimens were reproduced. During the loading and unloading consolidation phases, changes in σ_v' and the corresponding vertical strain ε_v were recorded. This allowed the calculation of the constrained modulus M_0 and the coefficient of earth pressure at rest K_0.

A summary of the general CC conditions at the end of consolidation is given in Table 1. During the expansion phase of the pressuremeter test the sample boundary conditions could be controlled; these are reported in Table 1. The possible boundary conditions are summarized in Fig. 11. The boundary condition which was most frequently used was constant vertical and horizontal stresses (BC1).

After sample stressing and the self-boring insertion when appropriate, the pressuremeter test was performed by expanding the membrane to a maximum cavity strain (ε_θ) of about 10%. Cavity strain is defined in terms of circumferential strain

$$\varepsilon_\theta = \Delta R/R_0 \quad (8)$$

Generally, before the beginning of the expansion phase, a relaxation time of 30–60 min in tests with ideal installation and 60–180 min in tests with self-boring installation was allowed.

Strain-controlled tests were performed at a strain rate of about 1%/min using an electronic strain control unit (SCU) supplied by Cambridge In-Situ Ltd. The SCU automatically adjusts the expansion pressure as a function of the output from the strain arms.

Generally, during each expansion phase two or three unloading-reloading (UR) loops, and during each contraction phase one or two reloading-unloading (RU) loops, were performed. The strain amplitude for each UR or RU loop was approximately 0·1–0·2%. Full details of the CC study were given by Bellotti *et al.* (1987).

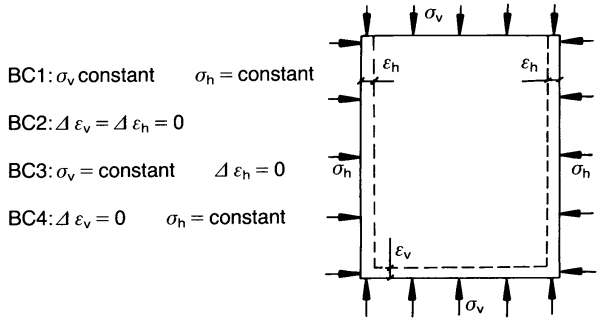

Fig. 11. Available boundary conditions in CC

Field study

SBPTs were performed at a site near the River Po, Italy (Bruzzi *et al.*, 1986). The site has a 20 m thick deposit of a relatively clean silica sand which is overlain by a 5–7 m deposit of clay silt. A geotechnical profile of the site, showing a summary of standard penetration test N_{SPT}, cone penetration test q_c and flat dilatometer test K_D data are presented in Fig. 12.

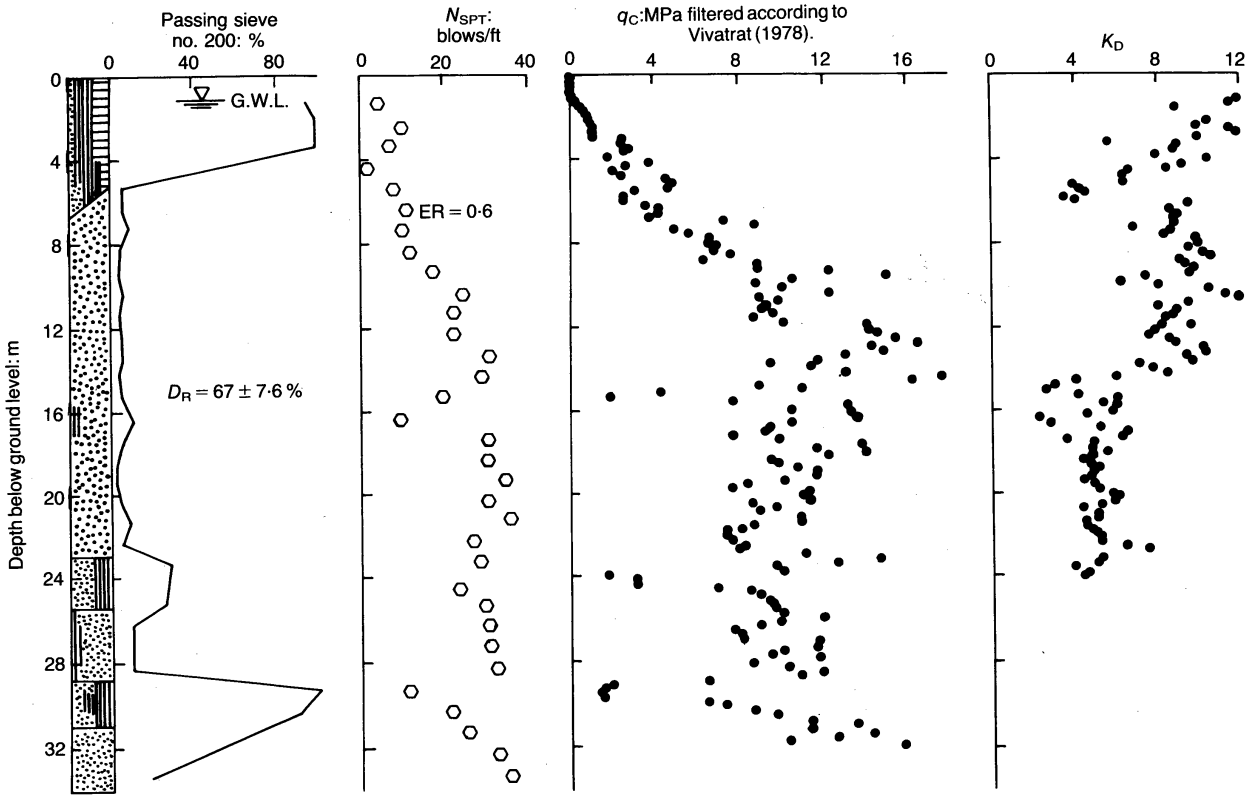

Fig. 12. Geotechnical profile at River Po site (borehole no. 4017)

Table 1. General calibration chamber conditions after sample consolidation

Installation type	Test	Sand	γ_d: kN/m^3	D_{Rc}: %	OC	σ_{v0}': kPa	σ_{h0}': kPa	K_0	u_0: kPa	M_0: MPa	No. of cycles		BC
											UR	RU	
Ideal	201	HS	16·08	67·0	2·77	112·8	74.56	0·662	0	192.18	2	1	1
	207	HS	15·22	43·9	3·29	109·9	64.75	0·586	0	185·51	2	1	1
	208	TS-4	14·82	43·2	1·00	112·8	45.13	0·400	0	34·14	2	1	1
	209	TS-4	15·01	49·2	1·00	116·7	51·99	0·441	0	43·56	3	1	1
	210	TS-4	15·13	53·3	1·00	511·1	244·27	0·479	0	100·06	3	1	1
	211	TS-4	15·57	67·4	1·00	512·1	242·31	0·473	0	114·88	3	2	1
	212	TS-4	15·49	64·6	2·86	110·9	82·40	0·747	0	189·82	3	1	1
	213	TS-4	14·96	47·5	2·78	112·8	83·39	0·740	0	168·63	3	1	1
	214	TS-4	14·80	42·4	1·00	113·8	53·96	0·476	0	50·82	3	1	4
	215	TS-4	16·42	92·3	1·00	514·6	225·63	0·439	0	143·72	3	1	1
	216	TS-4	14·92	46·3	7·57	60·8	56·90	0·927	0	156·76	3	1	1
	218	TS-4	15·51	65·4	7·66	59·8	59·84	0·980	0	169·62	3	1	1
	219	TS-4	15·52	65·9	5·46	112·9	101·04	0·902	0	207·48	3	1	1
	220	TS-4	14·95	47·2	1·00	313·3	150·09	0·481	0	80·15	3	1	1
	221	TS-4	14·87	44·6	2·88	108·9	81·42	0·751	0	167·36	3	1	1
	222	TS-4	14·92	46·2	5·50	111·8	95·16	0·850	0	199·05	3	1	1
	224	TS-4	15·81	74·6	5·38	113·8	93·20	0·816	0	222·39	3	1	1
	225	TS-4	15·81	74·6	5·46	111·8	87·31	0·775	0	218·27	3	—	1
	228	TS-4	15·89	77·0	1·00	518·0	215·82	0·417	0	120·27	3	1	1
	233	TS-4	15·98	79·6	1·00	512·1	224·65	0·439	0	121·25	3	1	1
	234	TS-4	15·93	76·1	5·34	115·8	103·99	0·904	0	216·21	3	1	1
	235	TS-4	14·99	48·5	1·00	516·0	239·36	0·465	0	80·54	3	—	1
	236	TS-4	15·83	75·2	2·72	114·8	78·48	0·686	0	190·41	3	1	1
Self-bored	237	TS-4	15·79	74·6	2·90	96·1	81·42	0·850	6·87	178·35	3	1	1
	238	TS-4	15·79	74·8	2·83	101·0	83·39	0·828	5·89	171·28	3	1	1
	239	TS-4	15·79	74·8	2·84	101·0	86·33	0·856	5·89	169·32	3	1	1
	240	TS-4	16·47	94·1	2·84	101·0	90·25	0·892	5·89	195·22	3	1	1
	241	TS-4	16·38	91·8	2·76	104·0	86·33	0·829	5·89	192·37	3	1	1
	242	TS-4	14·72	40·1	1·00	103·0	49·05	0·475	6·87	32·67	3	1	1
	243	TS-4	14·79	42·7	3·10	95·2	74·56	0·785	6.87	141·46	4	—	1
	244	TS-4	14·80	42·8	6·12	97·1	94·18	0·970	5·89	172·36	4	—	1
	245	TS-4	14·72	40·0	1·00	102·0	54·94	0·539	6·87	41·40	4	—	1
	246	TS-5	14·72	43·0	1·00	102·0	52·97	0·523	6·87	45·32	4	—	3
	247	TS-5	14·80	43·0	4·19	190·3	147·15	0·776	6·87	212·58	4	—	3
	250	TS-5	14·81	43·0	1·00	480·7	219·74	0·457	6·87	93·20	4	—	4
	251	TS-5	14·74	41·0	1·00	100·1	51·01	0·508	6·87	36·30	4	—	4
	252	TS-6	15·79	75·0	1·00	101·0	52·97	0·518	6·87	58·27	4	—	1
	253	TS-6	15·68	71·0	1·00	103·0	52·97	0·517	6·87	58·99	4	—	3
	254	TS-6	15·69	71·0	6·16	97·1	88·29	0·912	6·87	194·43	3	—	1
	255	TS-6	15·49	65·0	1·00	108·9	55·92	0·514	6·87	56·70	2	—	1
	256	TS-7	15·46	65·0	1·73	345·3	277·62	0·690	6·87	263·69	4	—	1
	257	TS-7	16·22	87·0	1·00	130·5	77·50	0·597	6·87	69·16	4	—	1
	258	TS-7	16·18	86·0	1·00	495·4	226·61	0·458	6·87	125·47	4	—	1
	259	TS-8	16·39	92·0	4·63	138·3	139·30	1·008	6·87	215·62	4	—	1
	260	TS-8	16·29	89·0	1·00	131·5	78·48	0·595	6·87	70·53	4	—	3
	261	TS-8	16·37	91·5	3·99	199·1	157·94	0·797	6·87	261·44	4	—	1
Ideal	262	TS-9	16·28	88·7	1·00	113·8	45·10	0·398	0	73·77	4	—	1
	263	TS-9	16·29	89·1	1·00	112·8	103·00	0·913	0	229·46	4	—	1

The SBPTs were performed using a Camkometer probe from England and a PAF-79 probe from France. The Camkometer and PAF-79 have L/D ratios of 6 and 4, respectively. Of all the performed tests, 25 good field SBPT results were evaluated as part of this study and were used for the analyses.

Test results

The measured unload-reload moduli G_{UR} were corrected to the in situ mean plane strain stress s_0', where

$$s_0' = \tfrac{1}{2}(\sigma_r' + \sigma_\theta') = \sigma_{h0}' \tag{9}$$

using

$$G_{UR}{}^{c} = G_{UR}\left(\frac{s_0'}{s_{AV}'}\right)^{n} \tag{10}$$

The value of $n = 0{\cdot}43$ was obtained from resonant column tests on Ticino sand (Lo Presti, 1987), and has been applied in this study. For the CC test results the in situ stress (σ_{h0}') was taken as the applied horizontal boundary stress. This was done to avoid confusion resulting from differences between in situ stresses (σ_{h0}') and pressuremeter lift-off stresses (p_0'). In general, the lift-off stresses were similar to the applied boundary stresses for the CC tests with ideal installation, but significantly different for tests with self-boring installation. It appears that the freshly deposited, unaged, uncemented, uniform, clean sand used in the CC creates particularly unfavourable conditions for the SBPT, especially for reliable assessment of in situ stress. It is believed that more reliable assessments of σ_{h0}' are possible in natural sands.

For the SBPTs in the River Po sand the in situ horizontal stresses were evaluated from the overall trend in measured lift-off stresses (Fig. 13). The results presented in Fig. 13 show that reasonable in situ coefficients of earth pressures K_0 were obtained using the Camkometer probe. However, unreasonably low values of K_0 were determined using the PAF-79. Due to the variation in measured lift-off stresses from each SBPT, the lift-off stresses obtained from the Camkometer were considered more reasonable and were used to evaluate the in situ horizontal stresses as shown in Fig. 13.

Tables 2–5 summarize the pertinent data and the values of G_{UR} and $G_{UR}{}^{c}$ for each of the unloading-reloading cycles in the SBPTs performed in the CC and at the River Po site. The small strain ($\gamma < 10^{-4}\%$) shear moduli G_0 obtained from resonant column tests $G_0{}^{RC}$ and cross-hole shear wave velocity measurements $G_0{}^{CH}$ are also included in the Tables.

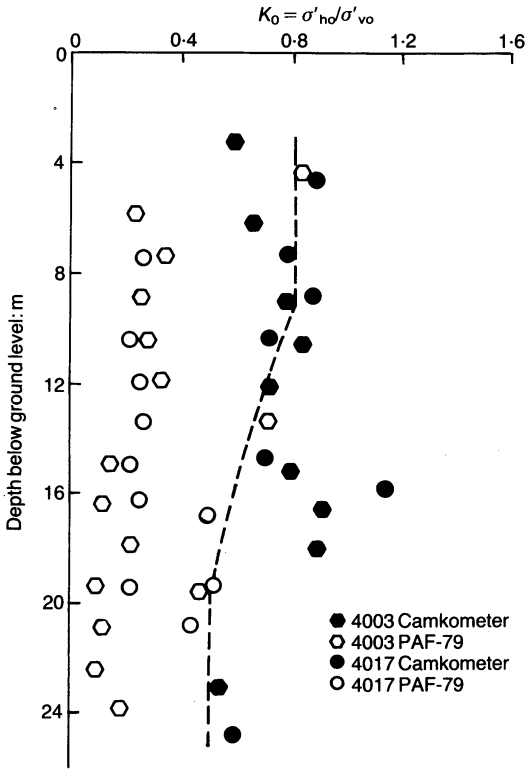

Fig. 13. Coefficient of earth pressure of River Po sand from SBP tests

The shear moduli $G_0{}^{RC}$ were obtained from resonant column tests performed by Lo Presti (1987) on pluvially-deposited Ticino sand. The value of $G_0{}^{RC}$ corresponding to each SBPT has been computed using the empirical equation based on the experimental data (Lo Presti, 1987)

$$G_0{}^{RC} = 591 p_a\left(\frac{\sigma_{mc}'}{p_a}\right)^{0{\cdot}426} \exp(0{\cdot}69 D_{Rc}) \tag{11}$$

where D_{Rc} is relative density of sand in CC after consolidation, p_a is reference stress (=98·1 kPa) and σ_{mc}' is mean effective consolidation stress.

Using the corrected $G_{UR}{}^{c}$ from the first UR cycle and the small strain shear modulus G_0 obtained at the same stress level, the ratio of the moduli are compared with the range of moduli reduction curves suggested by Seed, Wong, Idriss & Tokimatsu (1986) in Figs 14 and 15. The shear strain levels used to present the data in Figs 14 and 15 are one half of the calculated average shear strain amplitude in the plastic zone around the SBP probe γ_{AV}. The reduction of γ_{AV} by a factor of two is consistent with the Masing rule and the definition of single amplitude shear strain used to produce the curves by Seed *et al.* (1986).

Good agreement between the moduli ratio from the SBPT and the range suggested by Seed *et al.* (1986) can be seen in Figs 14 and 15. The scatter is a little larger for the field data. The

Table 2. SBPT data in calibration chamber with ideal installation

Test no.	Type	σ_{h_0}': kPa	ϕ_{PS}': °	p_c': kPa	ε_B: %	ε_A: %	α	γ_{AV}: %	G_{UR}: MPa	G_{UR}^c: MPa	G_0^{SBP}: MPa	G_0^{RC}: MPa
201	UR	74·6	49·1	266·8	1·141	1·018	0·178	0·120	47·2	40·3	83·7	81·9
	UR			438·5	2·974	2·855	0·193	0·080	50·7	38·6	69·7	
	RU			575·9	13·731	13·604	0·193	0·071	61·3	43·3	78·8	
207	UR	64·8	44·0	254·1	1·871	1·765	0·194	0·090	36·2	30·0	55·2	65·8
	UR			309·0	3·113	2·983	0·200	0·095	36·2	28·6	52·6	
	RU			306·1	9·502	9·376	0·200	0·093	43·9	34·8	66·8	
208	UR	45·1	39·1	128·1	1·096	0·990	0·183	0·113	25·2	22·3	45·0	56·1
	UR			154·0	1·810	1·711	0·199	0·088	27·4	23·2	44·1	
	RU			127·5	9·340	9·238	0·182	0·109	27·3	24·2	49·6	
209	UR	52·0	43·8	143·2	0·850	0·778	0·164	0·084	34·5	31·0	59·8	62·1
	UR			174·6	1·427	1·360	0·182	0·065	37·0	31·8	57·9	
	UR			225·6	2·619	2·550	0·198	0·054	40·8	33·0	58·4	
	RU			152·1	9·299	9·232	0·172	0·074	38·6	34·2	65·5	
210	UR	244·3	42·2	540·5	0·723	0·658	0·127	0·094	75·7	71·3	121·8	123·5
	UR			660·2	1·330	1·271	0·167	0·069	79·4	71·5	117·9	
	UR			779·9	2·098	2·032	0·185	0·066	79·4	68·8	112·5	
	RU			671·0	9·218	9·177	0·169	0·047	88·5	79·4	127·9	
211	UR	242·3	47·4	503·3	0·842	0·776	0·088	0·108	72·4	69·7	120·7	135·6
	UR			665·1	1·772	1·707	0·154	0·079	79·1	71·6	119·5	
	UR			828·0	2·949	2·882	0·178	0·067	81·5	70·1	114·8	
	RU			1287·1	9·705	9·638	0·195	0·047	100·9	78·1	125·3	
	RU			688·3	9·155	9·089	0·152	0·082	86·5	78·5	132·8	
212	UR	82·5	44·9	278·6	0·868	0·799	0·183	0·067	48·0	41·2	72·6	84·0
	UR			377·7	1·779	1·707	0·197	0·055	50·6	40·4	68·6	
	UR			493·4	3·198	3·124	0·200	0·046	52·3	39·1	64·9	
	RU			652·4	9·696	9·626	0·198	0·037	58·3	40·9	66·7	
213	UR	83·4	39·5	268·8	0·699	0·625	0·194	0·070	47·9	41·2	73·5	75·1
	UR			357·1	1·777	1·714	0·207	0·047	48·7	39·2	65·3	
	UR			421·8	2·871	2·803	0·210	0·044	51·4	39·7	65·9	
	RU			533·3	9·641	9·555	0·210	0·048	58·1	42·3	71·3	
214	UR	54·0	43·1	144·2	0·724	0·646	0·162	0·093	32·3	29·2	56·5	60·2
	UR			194·2	1·495	1·415	0·191	0·072	34·7	29·3	53·3	
	UR			244·3	2·482	2·404	0·201	0·058	36·9	29·5	51·5	
	RU			380·6	9·988	9·910	0·203	0·043	45·6	32·6	55·3	
215	UR	225·6	44·3	552·3	0·510	0·432	0·143	0·103	93·7	86·6	157·4	156·2
	UR			734·8	1·041	0·969	0·181	0·072	93·9	81·3	137·8	
	UR			911·4	1·694	1·628	0·194	0·055	105·9	87·1	144·2	
	RU			1580·4	9·713	9·643	0·201	0·039	122·0	87·5	140·8	
216	UR	56·9	36·7	215·8	0·803	0·735	0·211	0·053	41·0	33·8	59·4	63·3
	UR			265·9	1·551	1·487	0·216	0·042	42·1	32·9	55·8	
	UR			314·9	2·689	2·623	0·217	0·038	40·9	30·8	51·0	
	RU			401·2	9·591	9·515	0·215	0·038	47·2	33·3	55·6	
218	UR	59·8	39·5	263·9	0·910	0·832	0·208	0·056	45·9	36·6	65·3	63·7
	UR			321·8	1·567	1·498	0·211	0·043	46·1	35·0	59·4	
	UR			378·7	2·428	2·365	0·210	0·035	47·2	34·4	56·9	
	RU			509·1	10·161	10·095	0·260	0·031	55·1	37·2	61·1	
219	UR	101·0	41·0	351·2	0·618	0·538	0·195	0·072	61·6	52·2	94·3	92·5
	UR			446·4	1·266	1·190	0·205	0·056	61·4	49·1	84·1	
	UR			554·3	2·268	2·187	0·208	0·051	65·0	49·3	83·3	
	RU			620·0	9·995	9·933	0·207	0·036	78·5	57·9	95·8	

Table 2—*continued*

Test no.	Type	σ_{h0}': kPa	ϕ_{PS}': °	p_c': kPa	ε_B: %	ε_A: %	α	γ_{AV}: %	G_{UR}: MPa	G_{UR}^c: MPa	G_0^{SBP}: MPa	G_0^{RC}: MPa
220	UR	150·1	40·5	339·4	1·161	1·097	0·139	0·088	51·4	48·0	82·6	96·2
	UR			403·2	2·106	2·045	0·171	0·070	50·9	45·8	76·0	
	UR			474·8	3·431	3·364	0·189	0·066	54·2	46·9	77·6	
	RU			439·5	10·062	9·998	0·182	0·067	60·8	53·6	90·3	
221	UR	81·4	41·6	273·7	1·261	1·197	0·191	0·060	45·7	39·1	67·4	72·8
	UR			330·6	2·184	2·121	0·201	0·050	44·2	36·1	60·3	
	UR			389·5	3·321	3·259	0·205	0·044	48·7	38·3	63·2	
	RU			335·5	9·979	9·911	0·201	0·054	50·2	40·9	69·8	
222	UR	95·2	40·0	321·8	0·945	0·882	0·196	0·058	53·9	45·9	78·8	78·7
	UR			406·1	1·975	1·909	0·206	0·049	51·6	41·6	69·2	
	UR			487·6	3·329	3·264	0·209	0·042	51·6	39·8	64·8	
	RU			534·7	10·095	10·028	0·210	0·041	62·8	47·3	78·1	
224	UR	93·2	43·8	328·6	0·689	0·624	0·188	0·060	61·1	51·9	91·5	94·9
	UR			427·7	1·348	1·281	0·199	0·050	62·5	49·9	84·8	
	UR			522·0	2·218	2·154	0·202	0·041	58·7	44·5	73·8	
	RU			750·5	10·382	10·315	0·200	0·034	78·1	54·0	88·8	
225	UR	87·3	44·3	325·7	0·897	0·804	0·191	0·083	48·7	40·8	73·9	92·3
	UR			428·8	1·717	1·645	0·200	0·052	52·4	41·1	69·1	
	UR			513·1	2·637	2·569	0·201	0·043	54·3	40·7	67·0	
228	UR	215·8	44·3	456·2	0·573	0·506	0·106	0·104	67·3	64·2	111·6	138·0
	UR			555·3	0·937	0·870	0·152	0·084	70·8	64·7	109·2	
	UR			655·3	1·375	1·307	0·175	0·073	77·8	68·5	114·4	
	RU			1320·4	10·474	10·405	0·201	0·042	108·3	80·4	129·7	
233	UR	224·7	45·5	443·4	0·590	0·517	0·076	0·124	66·9	64·9	115·5	142·9
	UR			557·2	0·961	0·898	0·142	0·083	75·5	69·7	117·9	
	UR			676·9	1·442	1·373	0·171	0·076	78·7	69·6	116·2	
	RU			1319·5	8·684	8·619	0·199	0·042	109·3	82·2	132·1	
234	UR	104·0	43·3	322·8	0·609	0·539	0·180	0·072	53·6	46·8	82·2	100·5
	UR			533·7	2·058	1·994	0·202	0·044	63·1	49·4	81·6	
	UR			684·7	3·611	3·546	0·203	0·037	67·1	48·8	79·4	
	RU			663·2	8·306	8·221	0·203	0·055	71·2	52·2	88·2	
235	UR	239·4	41·5	422·8	0·656	0·588	0·040	0·126	64·0	63·2	111·5	118·4
	UR			670·0	2·196	2·129	0·174	0·075	68·9	61·5	101·0	
	UR			847·6	3·865	3·795	0·195	0·063	72·8	61·5	99·5	
236	UR	78·5	45·0	233·5	0·522	0·451	0·171	0·078	57·4	50·8	98·0	88·6
	UR			497·1	2·044	2·004	0·200	0·071	61·7	45·5	83·4	
	UR			535·6	3·652	3·564	0·200	0·051	64·6	46·7	80·8	
	RU			571·9	7·176	7·110	0·199	0·037	84·4	60·0	102·6	
262	UR	45·1	46·0	171·1	0·568	0·480	0·188	0·079	35·6	29·8	58·0	76·8
	UR			311·3	1·844	1·739	0·198	0·061	38·9	28·1	50·5	
	UR			451·0	3·723	3·615	0·193	0·051	39·9	26·2	45·0	
	RU			584·7	6·618	6·531	0·187	0·036	41·9	25·7	42·1	
263	UR	103·0	49·1	343·6	0·590	0·585	0·172	0·102	57·1	49·5	94·0	109·4
	UR			517·2	1·509	1·408	0·191	0·076	60·0	47·2	83·1	
	UR			693·0	2·771	2·656	0·193	0·070	63·0	46·1	79·8	
	RU			858·0	4·311	4·206	0·192	0·057	62·9	43·5	72·7	

Table 3. SBPT data in calibration chamber with self-bored installation

Test no.	Type	σ_{h0}': kPa	ϕ_{PS}': °	p_c': kPa	ε_B: %	ε_A: %	α	γ_{AV}: %	G_{UR}: MPa	$G_{UR}{}^c$: MPa	G_0^{SBP}: MPa	$G_0{}^{RC}$: MPa
237	UR	81·4	43·1	314·9	0·787	0·732	0·195	0·047	49·6	41·1	69·0	89·6
	UR			449·3	1·902	1·831	0·203	0·046	49·8	37·9	62·8	
	UR			554·3	3·061	2·977	0·203	0·047	51·3	37·0	61·4	
	RU			596·5	7·718	7·655	0·202	0·034	60·5	42·8	69·7	
238	UR	83·4	37·6	383·7	0·978	0·920	0·214	0·039	45·4	35·7	58·2	90·6
	UR			498·4	2·157	2·083	0·215	0·041	52·0	38·3	63·1	
	UR			545·4	3·350	3·250	0·214	0·053	50·6	36·4	61·2	
	RU			526·8	7·604	7·544	0·214	0·032	50·0	36·4	58·3	
239	UR	86·3	39·4	369·8	0·941	0·884	0·208	0·042	54·0	43·4	72·1	91·9
	UR			520·9	2·326	2·236	0·211	0·052	48·8	36·0	60·0	
	UR			629·8	3·790	3·672	0·209	0·060	46·8	32·9	55·1	
	RU			587·6	8·217	8·101	0·210	0·062	53·2	38·1	65·2	
241	UR	86·3	40·5	465·0	1·042	0·977	0·208	0·041	72·9	55·5	94·6	103·4
	UR			659·2	2·441	2·366	0·206	0·038	63·0	43·9	72·1	
	UR			813·3	3·956	3·862	0·202	0·042	61·6	40·6	66·8	
	RU			863·3	9·272	9·201	0·201	0·031	71·2	46·1	74·8	
242	UR	49·1	40·5	108·9	1·776	1·710	0·135	0·093	18·0	16·9	29·6	56·9
	UR			153·0	3·727	3·634	0·188	0·092	18·5	16·1	28·0	
	UR			186·4	5·922	5·805	0·201	0·097	18·5	15·3	26·7	
	RU			174·6	9·892	9·810	0·197	0·072	24·7	20·8	36·2	
243	UR	74·6	39·0	76·5	0·762	0·690	0	0·144	14·2	14·2	24·6	69·2
	UR			122·6	2·431	2·348	0·071	0·130	15·6	22·3	39·0	
	UR			154·0	4·477	4·394	0·169	0·098	16·8	21·8	36·5	
	UR			191·3	7·779	7·878	0·195	0·077	16·0	21·4	34·8	
244	UR	94·2	40·5	99·1	0·544	0·467	0	0·154	18·2	18·2	31·6	76·5
	UR			174·6	1·445	1·370	0·071	0·130	22·9	22·3	39·0	
	UR			249·2	3·483	3·399	0·169	0·098	24·2	21·8	36·5	
	UR			319·8	6·709	6·625	0·195	0·077	25·1	21·4	34·8	
245	UR	54·9	47·4	105·8	0·557	0·476	0·058	0·144	15·1	14·8	26·6	59·6
	UR			196·5	2·300	2·214	0·181	0·083	22·1	18·8	32·1	
	UR			224·2	2·561	2·396	0·188	0·142	17·3	14·3	25·5	
	UR			270·1	5·997	5·798	0·194	0·148	17·0	13·4	23·8	
246	UR	58·0	39·9	132·1	0·782	0·692	0·162	0·111	18·6	17·0	30·4	60·0
	UR			196·5	2.300	2·214	0·201	0·072	22·1	18·4	31·2	
	UR			245·6	4·214	4·090	0·208	0·087	22·3	17·6	30·4	
	UR			303·9	7·411	7·317	0·210	0·056	25·4	19·0	31·4	
247	UR	147·2	48·6	168·5	1·034	0·955	0	0·158	26·7	26·7	55·4	92·7
	UR			310·7	2·389	2·296	0·090	0·151	33·9	32·6	57·0	
	UR			450·3	4·226	4·134	0·165	0·103	38·0	33·6	56·1	
	UR			592·0	6·573	6·476	0·185	0·086	42·6	35·3	58·1	
250	UR	219·7	42·0	601·8	1·000	0·929	0·169	0·082	61·5	56·2	91·2	109·9
	UR			790·2	2·512	2·433	0·194	0·070	62·5	52·1	85·5	
	UR			978·5	4·516	4·432	0·203	0·063	63·1	50·5	81·0	
	UR			1163·6	7·069	6·989	0·205	0·052	66·3	50·9	80·7	
251	UR	51·0	44·3	66·1	1.135	1·044	0	0·182	12·7	12·7	23·8	58·2
	UR			98·9	2·741	2·665	0·074	0·130	15·0	14·6	26·2	
	UR			129·0	5·209	5·125	0·149	0·108	16·1	14·8	25·7	
	UR			154·8	7·995	7·907	0·175	0·094	17·4	15·3	26·3	
252	UR	53·0	41·6	242·8	0·916	0·836	0·205	0·057	34·6	27·4	47·5	74·8
	UR			341·3	2·218	2·136	0·206	0·046	35·1	25·5	42·5	
	UR			436·9	4·029	3·951	0·203	0·038	36·7	25·0	40·8	
	UR			529·7	6·626	6·541	0·199	0·037	36·9	23·9	39·0	

Table 3—*continued*

Test no.	Type	σ_{h0}': kPa	ϕ_{PS}': °	p_c': kPa	ε_B: %	ε_A: %	α	γ_{AV}: %	G_{UR}: MPa	G_{UR}^c: MPa	G_0^{SBP}: MPa	G_0^{RC}: MPa
253	UR	53·0	51·8	208·7	1·079	0·995	0·178	0·078	31·5	26·4	47·3	72·8
	UR			312·7	2·176	2·059	0·189	0·080	34·1	25·9	46·5	
	UR			416·9	3·562	3·473	0·189	0·051	36·7	25·9	43·4	
254	UR	88·3	49·8	229·0	0·761	0·680	0·138	0·107	35·5	32·7	58·9	90·4
	UR			425·7	2·071	1·985	0·189	0·067	42·4	33·7	56·8	
255	UR	55·9	44·3	218·3	0·872	0·784	0·193	0·075	36·4	30·2	55·2	71·4
	UR			321·1	2·207	2·127	0·201	0·051	37·6	28·4	48·1	
	UR			421·2	3·952	3·868	0·200	0·045	39·7	27·9	46·6	
	UR			525·5	6·205	6·128	0·196	0·036	43·8	29·1	47·6	
256	UR	277·6	41·6	351·3	0·696	0·611	0	0·170	49·1	49·1	72·7	141·4
	UR			504·4	1·796	1·716	0·055	0·144	56·1	55·1	94·8	
	UR			657·1	3·443	3·356	0·145	0·116	57·4	53·2	88·7	
	UR			845·4	5·762	5·612	0·183	0·093	54·5	47·7	77·1	
257	UR	77·5	44·3	222·8	0·552	0·463	0·169	0·100	37·7	33·6	62·4	95·5
	UR			370·9	2·021	1·941	0·199	0·058	42·4	33·5	56·6	
	UR			493·2	4·171	4·081	0·201	0·054	42·4	31·2	51·7	
	UR			598·9	7·076	6·985	0·200	0·048	40·5	28·3	46·1	
258	UR	226·6	49·0	406·6	0·557	0·474	0·014	0·162	60·3	60·0	110·2	149·8
	UR			685·0	1·223	1·141	0·163	0·093	73·8	65·5	111·0	
	UR			959·8	2·201	2·114	0·187	0·074	78·0	64·0	105·3	
	UR			1240·0	3·504	3·421	0·193	0·058	87·1	67·1	108·6	
259	UR	139·0	44·3	432·6	0·774	0·628	0·177	0·153	52·0	45·5	87·6	121·7
	UR			594·0	1·731	1·631	0·196	0·088	53·9	43·8	74·8	
	UR			754·2	2·932	2·837	0·201	0·063	59·0	45·2	74·5	
	UR			923·6	4·434	4·344	0·201	0·052	58·6	42·6	68·8	
260	UR	78·5	44·0	262·0	0·861	0·771	0·184	0·088	37·0	31·8	56·7	97·4
	UR			382·6	1·971	1·873	0·200	0·070	40·7	32·0	54·9	
	UR			503·6	3·278	3·184	0·202	0·056	42·8	31·4	52·2	
	UR			625·9	4·854	4·764	0·200	0·047	46·4	32·2	52·7	
261	UR	157·9	46·7	438·8	0·529	0·447	0·158	0·098	63·4	57·2	103·4	133·5
	UR			715·6	1·376	1·289	0·193	0·068	70·7	56·8	95·4	
	UR			1012·5	2·752	2·667	0·197	0·052	72·0	53·1	86·2	
	UR			1336·8	4·517	4·437	0·195	0·041	74·3	51·0	81·2	

Table 4. SBPT data at the River Po site with Camkometer probe

Depth m	Type	σ_{h0}': kPa	ϕ_{PS}': °	p_c': kPa	ε_B: %	ε_A: %	α	γ_{AV}: %	G_{UR}: MPa	G_{UR}^c: MPa	G_0^{SBP}: MPa	G_0^{CH}: MPa
7·4	UR	58·0	36·3	206·7	0·56	0·44	0·209	0·098	25·0	20·9	37·5	42·0
	UR			260·4	1·14	1·04	0·217	0·067	27·0	21·3	36·2	
	RU			239·4	9·79	9·66	0·215	0·094	26·9	21·7	38·9	
	RU			188·4	9·51	9·37	0·204	0·125	23·6	20·2	37·9	
8·9	UR	68·0	42·1	248·3	0·60	0·51	0·195	0·079	35·5	29·8	53·0	46·5
	UR			304·1	0·99	0·89	0·203	0·075	34·6	27·7	48·1	
	UR			366·3	1·51	1·42	0·205	0·058	36·7	28·0	47·1	
	RU			284·5	9·32	9·19	0·201	0·102	33·4	27·1	49·8	
10·4	UR	75·1	36·7	278·6	0·82	0·73	0·210	0·072	27·9	23·1	38·6	60·4
	UR			344·4	1·40	1·32	0·216	0·053	30·3	23·8	38·8	
	RU			254·1	9·62	9·51	0·205	0·095	29·8	25·2	44·5	
11·9	UR	79·9	36·7	332·0	0·75	0·65	0·214	0·072	33·0	26·6	44·9	63·8
	UR			385·1	1·14	1·04	0·216	0·064	35·9	27·9	46·7	
	UR			429·5	1·69	1·60	0·217	0·053	38·4	29·0	47·9	
	RU			355·4	9·56	9·46	0·215	0·068	38·8	30·7	52·6	
13·4	UR	82·7	35·0	607·1	1·01	0·92	0·218	0·042	56·2	39·0	64·5	68·1
	UR			722·2	2·08	1·99	0·214	0·038	54·3	36·3	59·0	
	RU			575·8	9·54	9·44	0·218	0·048	56·3	39·7	66·9	
14·8	UR	82·5	36·0	508·2	2·66	2·54	0·218	0·064	40·8	29·7	50·1	77·7
	UR			604·3	4·35	4·39	0·216	0·029	45·7	31·8	50·4	
	UR			698·5	6·21	6·11	0·213	0·044	43·6	29·2	47·3	
15·9	UR	86·6	34·5	433·8	0·57	0·49	0·222	0·048	48·4	37·0	61·6	81·6
	UR			530·2	1·20	1·11	0·221	0·047	49·2	35·8	59·1	
	UR			596·2	1·85	1·76	0·220	0·043	49·9	35·2	57·7	
17·9	UR	88·6	35·8	399·3	0·59	0·53	0·218	0·040	48·1	37·9	61·8	89·6
	UR			485·6	1·30	1·22	0·219	0·046	50·3	37·7	62·4	
	UR			561·2	2·26	2·19	0·218	0·036	56·4	40·8	66·5	
	RU			465·0	9·70	9·61	0·219	0·053	59·5	45·1	77·7	
19·4	UR	90·2	35·5	397·8	0·71	0·64	0·218	0·047	48·0	38·0	62·9	98·0
	UR			493·5	1·60	1·52	0·220	0·046	48·0	36·0	59·1	
	RU			477·8	9·81	9·73	0·220	0·047	57·8	43·7	73·5	
20·9	UR	93·0	37·1	466·4	0·51	0·45	0·216	0·038	58·8	45·2	74·2	102·4
	UR			559·7	1·01	0·94	0·216	0·039	60·7	44·6	73·3	
	UR			645·5	1·71	1·63	0·214	0·040	62·9	44·6	73·5	
	RU			537·6	9·59	9·50	0·216	0·051	70·1	52·1	90·1	
22·8	UR	101·0	34·5	508·2	0·63	0·58	0·222	0·030	60·0	45·9	73·6	115·1
	UR			551·3	0·88	0·81	0·222	0·039	64·5	48·3	79·6	
	UR			590·6	1·19	1·13	0·222	0·032	59·5	43·8	70·4	
	RU			531·7	9·46	9·38	0·222	0·046	65·8	49·7	83·7	
24·8	UR	108·3	34·0	369·9	0·57	0·50	0·215	0·057	49·0	41·0	68·8	105·9
	UR			417·0	0·92	0·84	0·219	0·058	48·6	39·6	66·3	
	UR			461·1	1·38	1·30	0·222	0·054	44·8	35·7	58·5	
	RU			727·0	9·53	9·45	0·221	0·039	52·5	37·3	59·8	

Table 5. SBPT data at the River Po site with PAF-79 probe

Depth: m	Type	σ_{h0}': kPa	ϕ_{PS}': °	p_c': kPa	ε_B: %	ε_A: %	α	γ_{AV}: %	G_{UR}: MPa	G_{UR}^c: MPa	G_0^{SBP}: MPa	G_0^{CH}: MPa
7·5	UR	58·7	51·9	147·2	1·634	1·462	0·126	0·240	16·8	15·6	32·0	42·4
9·0	UR	68·7	53·7	407·1	3·312	3·083	0·187	0·160	38·7	29·4	61·7	47·1
10·5	UR	75·7	57·3	263·9	1·651	1·461	0·161	0·205	28·5	24·7	51·0	60·1
	UR			366·9	3·209	3·084	0·178	0·104	34·6	27·8	49·3	
12.0	UR	79·8	55·0	278·6	1·662	1·461	0·165	0·212	31·7	27·4	58·9	64·5
13·5	UR	82·7	53·8	350·2	1·606	1·318	0·179	0·256	31·8	26·2	59·6	68·8
15·0	UR	84·8	55·2	323·7	1·654	1·460	0·171	0·191	34·0	28·8	59·0	80·8
	UR			470·9	3·269	3·082	0·184	0·138	40·5	31·4	59·6	
16·5	UR	88·1	55·5	499·3	3·319	3·082	0·184	0·174	41·6	32·1	65·0	86·0
18·0	UR	89·0	59·3	572·9	3·315	2·815	0·181	0·347	35·0	26·3	67·1	89·6
19·5	UR	87·2	59·3	407·1	1·623	1·391	0·175	0·201	41·0	33·3	72·4	98·0
21·0	UR	93·4	60·0	514·0	3·357	3·085	0·178	0·211	43·1	33·7	72·7	101·5
22·5	UR	99·7	60·0	432·6	1·663	1·459	0·171	0·188	45·9	38·0	80·0	114·1
	UR			613·1	3·304	3·085	0·180	0·157	54·3	41·2	83·8	
24.0	UR	104·5	60·0	463·0	1·698	1·458	0·172	0·218	44·2	36·4	78·5	115·0
27·0	UR	117·0	60·0	632·7	1·668	1·456	0·178	0·166	68·9	54·0	117·2	107·0
	UR			902·7	3·328	3·076	0·180	0·157	74·7	53·6	113·0	

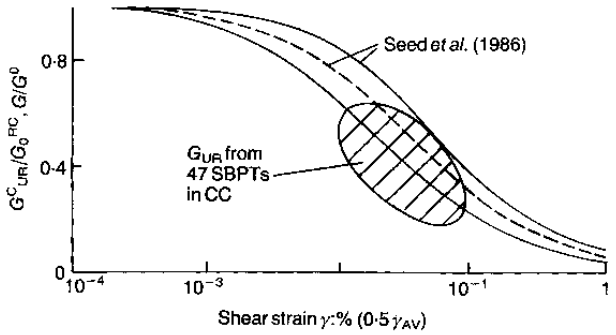

Fig. 14. Comparison between G_{UR}^c from CC (corrected for stress level) and G_0^{RC} from resonant column tests

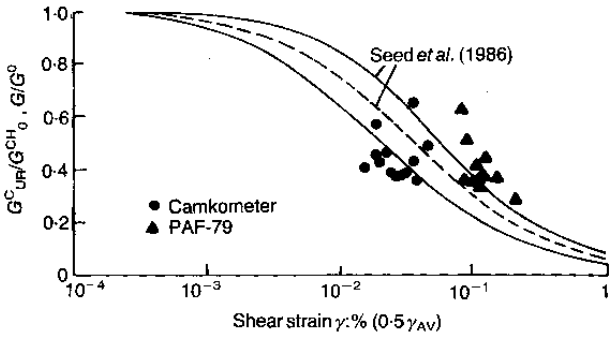

Fig. 15. Comparison between G_{UR}^c (corrected for stress level) and G_0^{CH} from cross-hole at River Po site

range of moduli ratios is similar to that found by Robertson and Hughes (1986) (Fig. 7).

A review of Tables 2–5 shows that as an approximation the average stress and strain around a SBP probe can be estimated by

$$s_{AV}' = p_0' + \alpha(p_c' - p_0') \tag{12}$$

$$\gamma_{AV} = \beta\Delta\gamma_c \tag{13}$$

where $\alpha \simeq 0{\cdot}2$ and $\beta \simeq 0{\cdot}5$. The value of $\beta \simeq 0{\cdot}5$ is the same as that suggested by Robertson (1982) and Robertson & Hughes (1986).

Although the correlations shown in Figs 14 and 15 look promising, there remain some important problems. The SBPT unload-reload moduli G_{UR} are determined after only one cycle of unloading-reloading (Fig. 6), whereas the resonant column and cross-hole seismic data are determined after many cycles ($N_c > 100$). Laboratory studies have shown that there is a difference in stiffness due to numbers of cycles (Ishibashi, 1974; Hardin and Drnevich, 1972; Ray, 1984). In principle, sands stiffen with increasing numbers of shear cycles. The amount of increase is dependent on shear strain amplitude and specimen density. Recent laboratory studies using a hollow cylinder torsional shear test apparatus combined with resonant column testing features (Guzman, 1986) have shown that a large difference can exist between the shear moduli measured after one

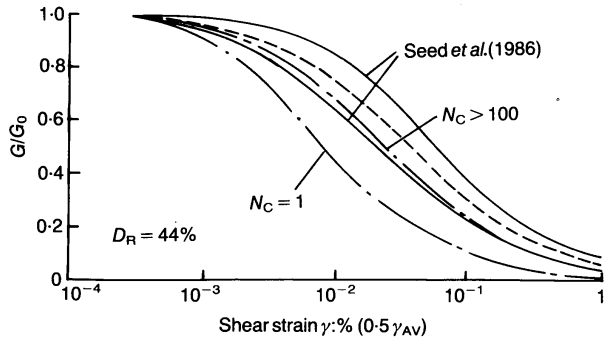

Fig. 16. Variation of G/G_0 with number of cycles N_c (after Guzman, 1986)

cycle and that recorded after many cycles for shear strains larger than 10^{-3}%. Fig. 16 presents a summary of these results (Guzman, 1986) compared with the range of moduli ratios suggested by Seed *et al.* (1986).

Guzman's results show that for strains less than the elastic threshold strain ($\gamma_t^e \simeq 10^{-3}$%) there appears to be no difference between the moduli for different numbers of cycles. However, the difference between the moduli at strains larger than the elastic threshold strain ($\gamma_t^e > 10^{-3}$%) is a function of shear strain level and probably void ratio (or relative density). At shear strains between 10^{-2} and 10^{-1}% the moduli for a large number of cycles ($N_c > 100$) can be as much as twice that recorded for one cycle. However, only limited data exist in the literature to confirm this observation. Available data indicate that the ratio of moduli varies from 1·25 to 2·0. The moduli ratio obtained by Guzman (1986) on Ottawa sand for a large number of cycles ($N_c > 100$) is consistent with the resonant column data from Seed *et al.* (1986).

The observed differences in G_{UR}^c within loops from the same SBPT can be attributed to

(a) differences in strain amplitude ($\Delta\gamma_c$)
(b) lack of precision in the definition of point B at the loop closure (see Fig. 6)
(c) creep occurring at the start of unloading, the amount of which depends on p_c'
(d) influence of disturbance (for self-bored tests) on the first UR loop, especially where $p_c' < \sigma_{h0}'(1 + \sin\phi_{PS}')$
(e) lack of precision in the strain measurements.

For a typical strain increment of $\Delta\gamma_c = 0{\cdot}2$% and probe diameter of 82 mm, the strain arms record a change in displacement of only 0·041 mm. For accurate measurement of the slope of the UR loop, a resolution in the displacement measurement of around 0·004 mm is required. The resolution of displacement measurement is affected by such factors as hysteresis, repeatability, linearity and stability of the displacement sensors signal. Fortunately, the strain arms generally showed good performance after the initial lift-off, as can be seen in Fig. 6.

An attempt was made to determine G_0 directly from the initial tangent modulus on unloading. However, due to limitations in precision of strain measurements the results were extremely erratic.

The proposed method for correcting SBPT data is based on the assumption that tests are performed in an infinite soil (i.e. in situ) and s_{AV}' and γ_{AV} are calculated within the plastic zone around the probe. The method for calculating γ_{AV} is consistent with that used to estimate s_{AV}'. Fahey (1980) demonstrated that because of the limited dimensions of some CCs, the slope of the pressure expansion curves obtained in the CC can be influenced by the boundary conditions. However, Fahey used a CC with a diameter of only 90 cm. In this study the limited dimensions of the ENEL-CRIS CC have been shown to have only a minor effect, resulting in a reduction in measured stiffness of less than 3%.

APPLICATION OF G_{UR} TO DESIGN

The proposed corrections for stress and strain level allow the moduli from SBPTs in sand (G_{UR}) to be compared with other moduli from either laboratory or in situ tests, with due consideration to stress and strain level. However, the application of G_{UR} to geotechnical design problems requires a further link. The type of link depends on the strain level expected in the design problem.

Figure 17 summarizes potential stress–strain

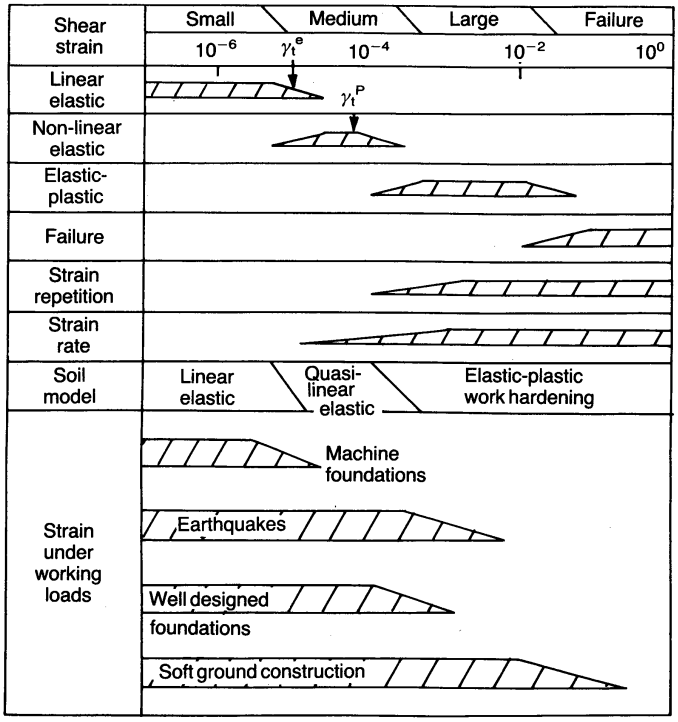

Fig. 17. Soil behaviour—constitutive models and deformation states

models, and relates them to their relevant strain levels of application. The figure is a simplification of the potential range of models available; however, it does provide a useful guide to the link between measured moduli (laboratory or in situ) and design problems.

Typically, for many dynamic or small-strain problems such as vibrating machine foundations and most well-designed statically loaded foundations, the required stress-strain relationship incorporates the low-strain moduli G_0 where $\gamma \leqslant 10^{-3}\%$. To link G_{UR} with G_0 it is necessary to use a relationship that can match the decay of G with increasing γ. One of the simplest solutions available is offered by the well-known hyperbolic stress-strain relation in the form proposed by Hardin & Drnevich (1972)

$$\frac{G}{G_0} = \frac{1}{1 + (\gamma/\gamma_r)} = \frac{1}{1 + (G_0\gamma/\tau_{max})} \qquad (14)$$

where G is shear modulus at shear strain γ, τ_{max} is maximum shear stress and γ_r is reference strain τ_{max}/G_0.

However, the above hyperbolic relationship was based on resonant column data where the number of cycles was large ($N_c > 100$). As shown in Fig. 16, the relationship for one cycle ($N_c = 1$) cannot be expected to fit the same hyperbolic relationship. Therefore, the SBPT G_{UR} requires a correction for number of cycles before the application of the above hyperbolic stress–strain relation.

To evaluate the approach suggested above, the CC and River Po SBPT data G_{UR} were converted to equivalent small strain moduli G_0^{SBP} as follows. First, the SBPT G_{UR} was corrected to an equivalent modulus $G_{UR}{}^c$ at the in situ mean plane strain stress. Second, $G_{UR}{}^c$ was increased by a factor F_N to allow for the number of cycles, using $(G_{UR}{}^c)_{N_c>100} = F_N(G_{UR}{}^c)_{N_c=1}$. As a first approximation, assume $F_N = 1{\cdot}5$ for $10^{-2} < \gamma < 10^{-1}\%$. The equivalent $G_{UR}{}^c$ for $N_c > 100$ was then corrected for strain level using the hyperbolic relationship

$$\frac{G_{UR}{}^c}{G_0^{SBP}} = \frac{1}{1 + (G_0^{SBP}\gamma_{AV}/2\tau_f)} \qquad (15)$$

where τ_f is SBPT shear stress at failure $= p_0' \sin \phi_{PS}'$.

The hyperbolic relationship proposed by Hardin & Drnevich (1972) represents the basic backbone or skeleton curve, as shown in Fig. 4. Since G_{UR} was measured during an unloading stage, τ_{max} must be taken as $2\tau_f$ to be consistent with the Masing rule.

The correction factor to allow for the number of cycles (F_N) has been assumed equal to 1·5. However, little data is available to ensure the validity of this value.

Comparisons between the equivalent SBPT small strain moduli G_0^{SBP} and the moduli from resonant column tests $G_0{}^{RC}$ and from cross-hole seismic tests $G_0{}^{CH}$ for the CC and River Po data are shown in Figs 18 and 19, respectively. Reasonably good agreement can be seen between the two moduli. Any lack of coincidence between $G_0{}^{RC}$, $G_0{}^{CH}$ and G_0^{SBP} may be due to

(*a*) the simplified and approximate nature of the proposed procedure to obtain G_0^{SBP} from G_{UR}
(*b*) possible variation in the factor F_N to account for the influence of number of cycles; variations in initial sand density may also influence the correction factor F_N
(*c*) possible influence of soil anisotropy.

Pluvially deposited sands tend to exhibit an anisotropic behaviour. Within the framework of the theory of elasticity for transversally isotropic (cross-anisotropic) soils, the available shear moduli can be defined as shear modulus for shearing in the horizontal plane $G_{UR} = G_{HH}$ and shear modulus for shearing in vertical plane $G_0{}^{RC}$, $G_0{}^{CH} = G_{VH}$. Large scale tests (Knox, 1982; Stokoe & Ni, 1985; Lee, 1986) indicate that $G_{HH}/G_{VH} = G_0^{SBP}/G_0{}^{RC} \simeq 1{\cdot}2$.

The proposed method requires a knowledge of ϕ_{PS}' to evaluate s_{AV}' and γ_{AV}. For the data shown in Tables 2–5 the values of ϕ_{PS}' were determined using the method proposed by Robertson & Hughes (1986). This method is a slight modification of that of Hughes, Wroth & Windle (1977). Small variations in ϕ_{PS}' have only a negligible

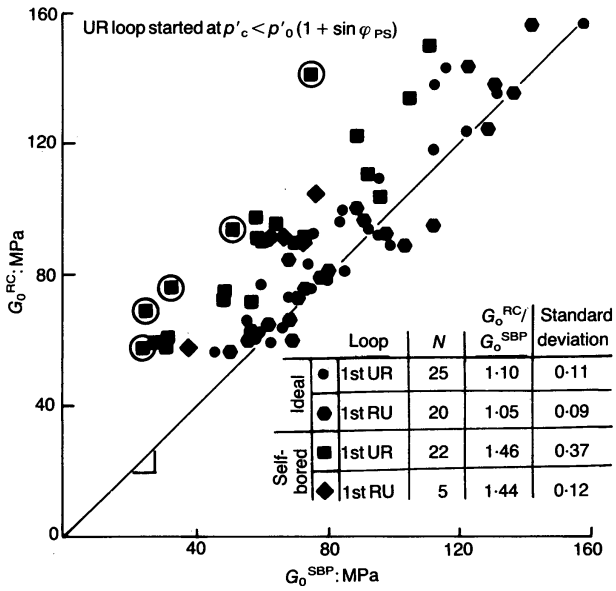

Fig. 18. G_0^{SBP} from unloading-reloading loop plotted against $G_0{}^{RC}$ from resonant column tests (SBPT performed in CC on Ticino and Hokksund sands)

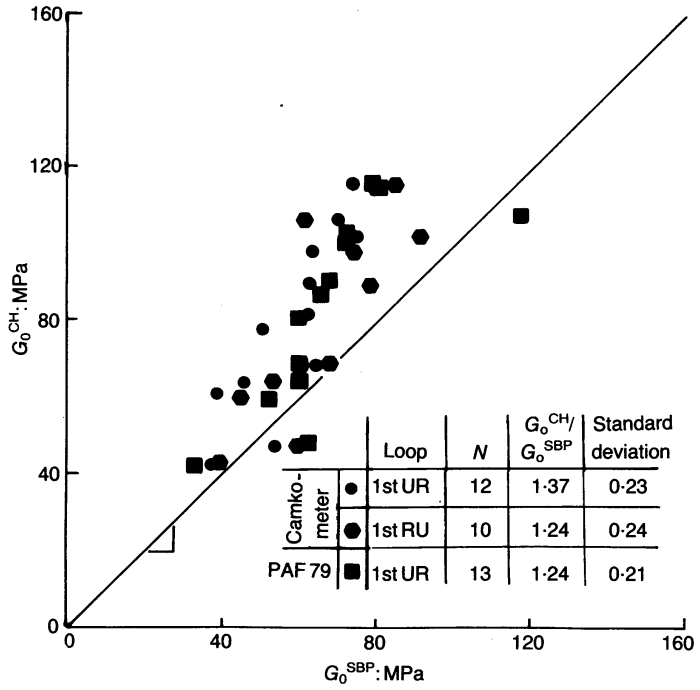

Fig. 19. G_0^{SBP} from unloading-reloading loop plotted against G_0^{CH} from cross-hole tests in River Po sand

influence on the value of $G_{UR}{}^c$ and G_0^{SBP}. However, variations in the value assumed for the in situ stress σ_{h0}' leads to a significant influence on the value of $G_{UR}{}^c$ and G_0^{SBP}.

Data presented in Fig. 17 show that when the UR loop is performed before a well-defined plastic zone has developed [$p_c' < p_0'(1 + \sin \phi_{PS}')$], the G_0^{SBP} values appear to be significantly underestimated. This is probably due to influence of disturbance in the early part of the test. These data also show that almost all of the values of G_0^{SBP} obtained from tests where the probe was installed by self-boring are underestimated compared with those obtained by ideal installation. Again, this is thought to be caused by disturbance due to the self-boring procedure in the CC.

The results obtained from self-bored tests in the field (Fig. 19) show a slight improvement over those obtained in the CC. The overall trend of σ_{h0}' from the SBPT field data and the calculated values of G_0^{SBP} appear to be reasonable and consistent.

For many static and larger strain design problems geotechnical engineers tend to have a preference to use Young's modulus E'. Since the SBPT moduli G_{UR} are measured during unloading, they represent, in principle, a stiffness of the sand below the current yield surface, and therefore implicitly apply only to OC sands that remain below their current yield surface during the anticipated loading.

To illustrate the importance of loading below the yield surface, it is possible to evaluate E' from G_0 and compare with laboratory-determined values of E' on both NC and OC samples. A series of drained, K_0 consolidated triaxial compression tests were performed on Ticino sand to measure E' as a function of strain. Using the relationship determined for Ticino sand (equation (11)) an equivalent value of G_0 was determined for the same densities and stress levels. Then, using the hyperbolic relationship in equation (14), it was possible to define a shear modulus at any strain level. These shear moduli values were converted to equivalent Young's moduli $E'(G^{RC})$ using the elastic relationship

$$E'(G^{RC}) = 2(1 - \nu')G \qquad (16)$$

where a value of Poisson's ratio $\nu' = 0{\cdot}2$ was assumed. The values of $E'(G^{RC})$ obtained from equation (16) were compared with the measured E' at the same stress and strain level. The comparison is summarized in Fig. 20. There is an excellent agreement between the measured E' and the equivalent $E'(G^{RC})$ determined from the resonant column tests for OC sand. The equivalent $E'(G^{RC})$ determined from resonant column tests are from unloading-reloading cycles, and therefore represent moduli below the yield surface. However, the measured E' for NC sand is considerably smaller than the equivalent $E'(G^{RC})$.

This example illustrates the importance of the following points.

(*a*) NC sands have a smaller stiffness than OC at the same stress and strain level.

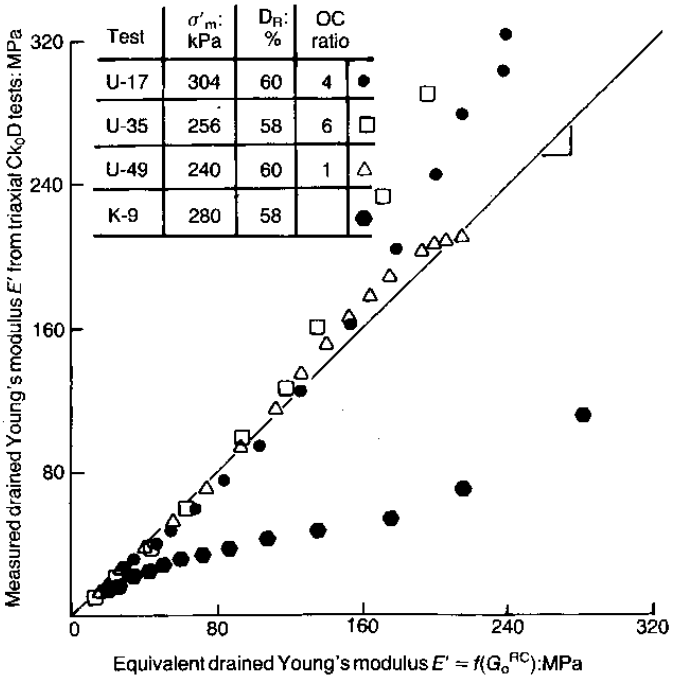

Fig. 20. Comparison between E' derived from laboratory triaxial CK_0D tests and $E'(G_0^{RC})$ for Ticino sand

(*b*) Moduli determined from unload-reload cycles implicitly apply only to OC sands that remain below their current yield surface.

The latter point implies that the G_{UR} values determined from SBPTs in sand only apply to the behaviour of the sand in an OC state below the current yield surface.

Many natural sand deposits have traditionally been considered to be normally consolidated. However, considerable evidence exists to suggest that most natural sands with an age greater than about 3000 years behave as overconsolidated sands for most loading conditions. This is probably due to one or more of the following factors

(*a*) aging
(*b*) cementation
(*c*) stress or strain history.

These same factors have been recognized for some time to produce a similar apparent preconsolidation in many clay soils.

The phenomenon of aging has also been recently recognized in the interpretation of penetration tests, such as the standard penetration test (Skempton, 1986) and the cone penetration test (Jamiolkowski, Ghionna, Lancellotta & Pasqualini, 1988).

CONCLUSIONS

A method has been proposed to correct the unload-reload moduli (G_{UR}) measured during a drained SBPT in sand to account for variations in stress and strain levels. The method assumes a simplified elastic perfectly plastic sand behaviour, and is based on the calculated average stress level within the plastic zone that existed around the probe before unloading and the average elastic strain level in the same area during the unloading cycle. The method has been evaluated using 47 SBPTs performed in the ENEL-CRIS calibration chamber (Bellotti *et al.*, 1987) and 25 SBPTs performed in a natural sand deposit at the Po River site in Italy (Bruzzi *et al.*, 1986). The values of G_{UR} were scaled to small strain and compared with the small strain moduli determined from resonant column tests G_0^{RC} and field cross-hole tests G_0^{CH}. A good agreement was observed. However, the following comments can be made.

(*a*) The shear stiffness of a sand is a complex function of void ratio, effective stress, shear strain, number of cycles, anisotropy and plasticity.
(*b*) The initial shear moduli G_i and secant shear moduli G_s are both sensitive to disturbance and are complex to locate within the framework of elasto-plastic theory. Therefore, G_i and G_s are almost impossible to link to other laboratory and in situ tests and to design problems.
(*c*) The shear moduli determined from unload-reload cycles G_{UR} can be considered as elastic but non-linear and are generally much less sensitive to disturbance due to installation. However, disturbance can influence G_{UR} if the UR cycle is performed before a well-defined

plastic zone has developed around the probe, i.e. $p_c' < p_0'(1 + \sin \phi_{PS}')$.

(*d*) G_{UR} should be linked to the relevant design problems via appropriate corrections accounting for stress and strain level. Soil anisotropy should also be considered, since SBPT $G_{UR} = G_{HH}$, whereas in many practical problems the value of G_{VH} is often more appropriate.

(*e*) Because G_{UR} reflects the shear stiffness of the sand below the current yield surface, in principle it refers only to the sand in the overconsolidated state.

(*f*) When relating G_{UR} to the small strain shear modulus (G_0^{RC}, G_0^{CH}) the influence of numbers of cycles should be considered before adjusting for strain level.

(*g*) Further work and evaluation is required to improve the link between measured G_{UR} and the stiffness required for specific design problems.

Further important factors in the determination of G_{UR} from pressuremeter tests in sand are related to the accuracy of the strain measurements and the test procedures. Since the values of G_{UR} are often large, the strain amplitude during unloading–reloading cycles is often small. Therefore, considerable attention to probe design is required for reliable strain measurements.

Although the above comments appear to reduce the usefulness of G_{UR} for engineering design, it should be remembered that G_{UR} represents a rather unique method to assess directly a shear stiffness for natural sands in situ. One of the main alternatives for a reliable assessment of moduli is the in situ measurement of shear wave velocity.

A potential area for further research is in the interpretation and application of the observed creep deformation during pressuremeter tests in sand. As the stress level increases during a pressuremeter test in sand there can be a significant increase in the amount of creep deformation. Therefore, procedures for performing unload-reload cycles should account for these creep deformations.

Although this Paper has addressed the interpretation of G_{UR} from self-boring pressuremeter tests, the approach can also be extended to results from other pressuremeter tests in sand, i.e. prebored and full-displacement. However, assumptions are required regarding the initial distribution of stresses around the pressuremeter probe before expansion.

ACKNOWLEDGEMENTS

The Authors would like to acknowledge the partial financial support and assistance for the calibration chamber studies from the US Army Research Office, USA contract number DAJA45-84-C-0034. Valuable comments and discussions with Professor K. H. Stokoe II and Professor R. Lancellotta concerning some of the topics is also appreciated. The Authors would also like to acknowledge the support provided by ENEL-CRIS, Milan, ISMES of Bergamo, Technical University of Torino, University of British Columbia and the Natural Sciences and Engineering Research Council of Canda.

APPENDIX 1. AVERAGE STRESS AND STRAIN ON HORIZONTAL PLANE IN PLASTIC ZONE AROUND EXPANDING CAVITY

The average mean effective stress at the start of the unloading-reloading loop is given by

$$s_{AV}' = \frac{\int_a^{R_p} s' \frac{dr}{r}}{\int_a^{R_p} \frac{dr}{r}} = \frac{\left(\frac{1}{2 \sin \phi_{PS}'} - \frac{p_0'}{p_c'} \frac{1 + \sin \phi_{PS}'}{2 \sin \phi_{PS}'}\right) p_c'}{\ln \left\{ \left[\frac{p_c'}{p_0'(1 + \sin \phi_{PS}')} \right]^{1 + \sin \phi_{PS}'/2 \sin \phi_{PS}'} \right\}} \quad (17)$$

where a is the cavity radius at start of loop and R_p is the radius of plastic zone at start of loop.

The average elastic shear strain during the unloading–reloading loop is given by

$$\gamma_{AV} = \frac{\int_a^{R_p} \frac{\Delta\gamma}{r} dr}{\int_a^{R_p} \frac{dr}{r}} = \frac{1}{2} \Delta\gamma_c \frac{\left[1 - \left(\frac{a}{R_p}\right)^2\right]}{\ln \frac{R_p}{a}} \quad (18)$$

where

$$\frac{R_p}{a} = \left[\frac{p_c'}{p_0'(1 + \sin \phi_{PS}')} \right]^{1 + \sin \phi_{PS}'/2 \sin \phi_{PS}'} \quad (19)$$

$$\Delta\gamma_c = 2(\varepsilon_B - \varepsilon_A) \quad (20)$$

ε_A and ε_B are the cavity strains at points A and B (Fig. 1).

REFERENCES

Baguelin, F., Jezequel, J. F. & Shields, D. H. (1978). *The pressuremeter and foundation engineering.* Series on Rock and Soil Mechanics. Clausthall: Trans. Tech. Publications.

Baldi, G., Bellotti, R., Crippa, V., Fretti, C., Ghionna, V. N., Jamiolkowski, M., Ostricati, D., Pasqualini, E. & Pedroni, S. (1985). Laboratory validation of in-situ tests. *AGI Golden Jubilee Vol. Geotech. Eng. in Italy, 11th ICSMFE, San Francisco,* 251–270.

Bellotti, R., Bizzi, G. & Ghionna, V. N. (1982). Design construction and use of a calibration chamber. *Proc. 2nd Eur. Symp. Penetration Test, Amsterdam* **2.**

Bellotti, R., Crippa, V., Ghionna, V. N., Jamiolkowski, M. & Robertson, P. K. (1987). *Self-boring pressuremeter in pluvially deposited sands.* Final Technical Report to US Army, European Research Office, London.

Bruzzi, D., Ghionna, V. N., Jamiolkowski, M., Lancellotta, R. & Manfredini, G. (1986). Self-boring pressuremeter in Po River sand. *Proc. 2nd Int. Symp. pressuremeter and its marine applications, Texas,* STP 950. Austin, American Society for Testing and Materials, 57–73.

Campanella, R. G. & Robertson, P. K. (1984). A seismic cone penetrometer to measure engineering properties of soil. *Proc. 54th Ann. Mtg Soc. Exploration Geophysicists, Atlanta.*

Dobry, R., Powell, D. J., Yokel, F. Y. & Ladd, R. S. (1980). Liquefaction potential of saturated sand—the stiffness method. *Proc. 7th Wld Conf. Earthquake engng, Istanbul* **3**, 25–32.

Fahey, M. (1980). *A study of the pressuremeter test in dense sand.* PhD thesis, Cambridge University.

Fahey, M. & Randolph, M. F. (1984). Effect of disturbance on parameters derived from self-boring pressuremeter tests in sand. *Géotechnique,* No. 1, 81–97.

Guzman, A. A. (1986). *Cyclic stress-strain and liquefaction characteristics of sands.* PhD thesis, Purdue University.

Hardin, B. O. & Drnevich, V. P. (1972). Shear modulus and damping in soils: design equations and curves. *J. Soil Mech. Fdns Div. Am. Soc. Civ. Engrs,* SM 7, 667–692.

Houlsby, G. T., Clarke, B. G. & Wroth, C. P. (1986). Analysis of the unloading for a pressuremeter in sand. *Proc. 2nd Int. Symp. pressuremeter and its marine applications, Texas.* American Society for Testing and Materials.

Hughes, J. M. O. (1982). Interpretation of pressuremeter tests for the determination of elastic shear modulus. *Proc. Engng Fdn Conf. Updating subsurface sampling of soils and rocks and their in-situ testing, Santa Barbara,* 279–289.

Hughes, J. M. O., Wroth, C. P. & Windle, D. (1977). Pressuremeter tests in sands. *Géotechnique* **27,** No. 4, 455–477.

Ishibashi, J. (1974). *Torsional simple shear device, liquefaction and dynamic properties of sands.* PhD thesis, University of Washington.

Iwasaki, T., Tatsuoka, F., Tokida, K. & Yasuda S. (1978). A practical method for assessing soil liquefaction potential based on case studies at various sites in Japan. *Proc. 2nd Int. Conf. Microzonation for safer construction research and application,* 885–895.

Jacobsen, M. (1976). *On pluvial compaction of sand.* Report 9, Laboratoiert for fundering, Aalborg University, Denmark.

Jamiolkowski, M., Ghionna, V. N., Lancellotta, R. & Pasqualini, E. (1988). New correlations of penetration tests in design practice. *Proc. 1st Int. Symp. Penetration test., Orlando,* 263–296.

Jamiolkowski, M., Ladd, C. C., Germaine J. T. & Lancellotta, R. (1985). New developments in field and laboratory testing of soils. *Proc. 11th Int. Conf. Soil Mech., San Francisco,* 57–153.

Janbu, N. (1963). Soil compressibility as determined by oedometer and triaxial tests. *Proc. 3rd Eur. Conf. Soil Mech., Wiesbaden* **2,** 19–24.

Knox, D. P. (1982). *Effect of state of stress on velocity of low amplitude shear wave propagating along principal stress direction in dry sand.* PhD thesis, Texas University.

Lee, S. H. H. (1986). *Investigation on low amplitude shear wave velocity in anisotropic material.* PhD thesis, Texas University.

Lo Presti, D. (1987). *Mechanical behaviour of Ticino sand from resonant column tests.* PhD thesis, Politechnico di Torino.

Ray, R. P. (1984). *Changes in shear modulus and damping in cohesionless soils due to repeated loading.* PhD thesis, University of Michigan.

Robertson, P. K. (1982). *In-situ testing of soil with emphasis on its application to liquefaction assessment.* PhD thesis, University of British Columbia.

Robertson, P. K. & Hughes, J. M. O. (1986). Determination of properties of sand from self-boring pressuremeter test. *Proc. 2nd Int. Symp. on the pressuremeter and its marine applications, Austin, Texas.* American Society for Testing and Materials, 283–302.

Robertson, P. K., Campanella, R. G., Gillespie, D. & Rice, A. (1986). Seismic CPT to measure in-situ shear wave velocity. *J. Geotech. Engng Div., Am. Soc. Civ. Engrs,* **112,** No. 8, 791–803.

Seed, H. B., Wong, R. T., Idriss, I. M. & Tokimatsu, K. (1986). Moduli and damping factors for dynamic analyses of cohesionless soils. *J. Geotech. Engng Div., Am. Soc. Civ. Engrs,* GT 11, 1016–1032.

Skempton, A. W. (1986). Standard penetration test procedures and the effects in sands of overburden pressure, relative density, particle size, ageing and overconsolidation. *Géotechnique,* No. 3, 425–447.

Vivatrat, V. (1978). *Cone penetration in clays.* PhD thesis, MIT.

Stokoe, K. H. & Ni, F. H. (1985). Effects of stress state and strain amplitude on shear modulus of dry sand. *Proc. 2nd Symp. Interaction of non-nuclear munitions with structures, Panama City Beach,* 407–412.

Withers, N. J., Howie, J., Hughes, J. M. O. & Robertson, P. K. (1988). The performance and analysis of cone pressuremeter tests in sands. *Géotechnique.*

Wroth, C. P. (1982). British experience with the self-boring pressuremeter. *Proc. 1st Symp. pressuremeter and its marine applications, Paris.* Edition Technip, 143–164.

Wroth, C. P., Randolph, M. F., Houlsby, G. T. & Fahey, M. (1979). *A review of the engineering properties of soils with particular reference to the shear modulus.* Report CUED/D Soils TR75, Cambridge University.